



Optimal design of metallic corrugated sandwich panels with polyurea-metal laminate face sheets for simultaneous vibration attenuation and structural stiffness

Xin Wang^{a,c,f}, Xue Li^{b,c}, Zeng-Shen Yue^{a,c}, Run-Pei Yu^{a,c}, Qian-Cheng Zhang^{a,d,*}, Shao-Feng Du^f, Zhi-Kun Yang^f, Bin Han^e, Tian Jian Lu^{b,c,*}

^a State Key Laboratory for Strength and Vibration of Mechanical Structures, Xi'an Jiaotong University, Xi'an 710049, PR China

^b State Key Laboratory of Mechanics and Control of Mechanical Structures, Nanjing University of Aeronautics and Astronautics, Nanjing 210016, PR China

^c Nanjing Center for Multifunctional Lightweight Materials and Structures (MLMS), Nanjing University of Aeronautics and Astronautics, Nanjing 210016, PR China

^d Key Laboratory of Intense Dynamic Loading and Effect, Northwest Institute of Nuclear Technology, Xi'an 710024, PR China

^e School of Mechanical Engineering, Xi'an Jiaotong University, Xi'an 710049, PR China

^f State Key Laboratory of Smart Manufacturing for Special Vehicles and Transmission System, Baotou 014030, China

ARTICLE INFO

Keywords:

Optimal design
Vibration damping
Surrogate model
Sandwich panel
Polyurea elastomer

ABSTRACT

With attributes such as high stiffness, high damping and lightweight, laser-welded corrugated-core (LASCOR) sandwich panels with polyurea-metal laminate (PML) face sheets were envisioned as multifunctional sandwich constructions to meet the growing needs of loading bearing and vibration/noise suppression. The sensitivity of vibration damping characteristics of these novel sandwich panels was systematically investigated using a combined finite element-modal strain energy (FE-MSE) method, and their superiority over monolithic panels having equal mass was highlighted. Subsequently, the fidelity of using the surrogate modeling technique to approximate the damping loss factor of the sandwich panel was analyzed. Under the principles of cross-validation, the orthogonal polynomial model was found to provide the most accurate predictions among four widely used surrogate models. A high-efficiency optimization procedure factoring structural stiffness, damping loss, and weight of the sandwich panel was proposed by coupling the surrogate model and an optimization algorithm. For single-objective optimization, the total weight of the optimal sandwich panel decreased by around 7% compared with that of preliminary design. Meanwhile, the Pareto fronts obtained from multi-objective optimizations revealed significant enhancements of both damping loss factor/structural stiffness and specific damping loss factor/structural stiffness.

1. Introduction

Ultralight all-metallic sandwich constructions with periodic lattice cores possess versatile features that are technically important for innovating engineering structures [1]. They not only outperform monolithic/stiffened structures of the same mass in stiffness and strength, but also provide additional attributes, such as thermal transport [2], sound insulation/absorption [3], blast/impact resistance [4], anti-penetration [5]. With ever-rising need for passive vibration attenuation, structural damping has drawn burgeoning attention. For example, engineering structures (e.g., ship hulls, automotive bodies, pulse detonation engines, and the like) often serve in a vibration-rich

environment, which may lead to severe structural damage (induced by resonant vibration or high cycle fatigue) and even passenger discomfort. However, due to intrinsically low loss factor of most metal materials [6,7], all-metallic sandwich constructions do not work well in passively controlling undesirable external vibration. Thus, how to enhance the vibration and damping properties of all-metallic sandwich structures by modifying their face sheets and cores becomes a necessity.

Of particular relevance to the current study is the method of viscoelastic layer treatment [8,9], which has been envisioned as an effective approach to achieve higher structural damping. To date, the two most widely-used configurations are the base/viscoelastic/

* Corresponding authors at: State Key Laboratory for Strength and Vibration of Mechanical Structures, Xi'an Jiaotong University, Xi'an 710049, PR China (Q.-C. Zhang). State Key Laboratory of Mechanics and Control of Mechanical Structures, Nanjing University of Aeronautics and Astronautics, Nanjing 210016, PR China (T.J. Lu).

E-mail addresses: zqc111999@xjtu.edu.cn (Q.-C. Zhang), tjlu@nuaa.edu.cn (T.J. Lu).

<https://doi.org/10.1016/j.compstruct.2020.112994>

Received 22 June 2020; Revised 22 August 2020; Accepted 17 September 2020

Available online 22 September 2020

0263-8223/© 2020 Elsevier Ltd. All rights reserved.

base laminate with constrained layer damping (CLD) [8] and the viscoelastic/base laminate with free layer damping (FLD) [9]. The former exhibits a greater capacity for vibration attenuation due to transverse shear deformation of the viscoelastic layer, while the latter almost relies on both in-plane extension and compression deformation to dissipate vibration energy [10]. Theoretically, existing modelling efforts [11], e.g., the Guyader model [12,13], the RKU model [14] and the Lamb wave model [15], have broadened insights into physical mechanisms underlying the CLD treatment. Besides, the vibration and instability phenomena associated with layered structures could be accurately investigated via numerical tools [16–20]. More recently, the CLD treatment was introduced to construct a hybrid face sheet for all-composite lattice-core sandwich structures [21–23]: upon sandwiching the fiber-reinforced composite face sheet with thin viscoelastic layers, the damping and stiffness efficiency of the sandwich structure was dramatically improved. However, thus far, few studies concerned the vibration/damping characteristics of all-metallic sandwich panels with 2D/3D lattice truss cores. This deficiency was squarely addressed in our prior study by replacing the monolithic metallic face sheets with polyurea-metal laminate (PML) ones [24].

Upon our recent work [24], novel laser-welded corrugate-core (LASCOR) sandwich panels with polyurea-metal laminate (PML) face sheets were fabricated, tested and numerically simulated using the method of finite element - modal strain energy (FE-MSE). Results demonstrated remarkable improvement of damping loss factors, quantitatively by as large as 10 times. However, a decline in natural frequencies was also observed, implying undesirable variation of structural stiffness and weight. In recent years, multifunctional sandwich constructions with high stiffness, lightweight and other functionalities (e.g., vibration damping, heat dissipation, energy absorption) have become increasingly attractive. To date, previous literatures as well as our own work have mainly focused on exploring the structural novelty and damping mechanisms of lattice-cored sandwich structures, with little attention devoted to setting up an optimization framework for simultaneous vibration attenuation and structural stiffness. For example, while both damping and stiffness efficiency of all-composite lattice-core sandwich structures were accounted for by Yang et al. [25], they did not carry out the corresponding multi-objective optimization; the optimization of Aumjaud et al. [26,27] focused on vibration damping and added mass of novel DSLJ-inserted honeycomb-core sandwiches, but not structural stiffness. Therefore, multi-objective optimization combining stiffness, damping, and weight of all-metallic lattice-core sandwich panels remains elusive.

Recently, incorporating the technique of surrogate modeling with optimization algorithms has advanced the applications of multi-objective optimal designs [28,29]. On one hand, coupling optimization algorithm with full numerical simulation usually requires a large amount of computational effort, burdens a high risk of premature simulation crash, and thus may be inefficient. On the other hand, deriving an exact equation to express the highly nonlinear relationship between a specific design objective and design variables is often difficult. Based on the principle of sampling estimation, the surrogate modeling technique is expected to overcome the above two barriers of optimal designs by bridging design objectives and variables. Nowadays, the commonly used surrogate models (sometimes also called machine learning models) include response surface (RS), radial basis function (RBF), kriging (KRG), orthogonal polynomial (OP), artificial neural network (ANN), support vector regression (SVR), and so on. For instance, concerning the optimization of sandwich structures, the RS model was implemented into the multi-objective optimal design of peak force and specific energy absorption for all-metallic truncated conical sandwich shells with corrugated cores [30], while the KRG model was adopted to develop a optimization scheme of blast resistance and structural weight for foam-core sandwich panels [31].

In this work, surrogate modeling was also selected to perform the multi-objective, multi-variable optimization task. The scope was to provide a comprehensive understanding of novel LASCOR sandwich panels with PML face sheets: (i) sensitivity of natural frequencies and damping loss factors to key geometric parameters, (ii) accuracy of surrogate model for the first damping loss factor, and (iii) multi-objective optimization framework of simultaneous vibration attenuation and structural stiffness with key geometric parameters as design variables. The paper was organized as follows. Section 2 reviewed briefly experiments carried out in our previous work [24]. Section 3 introduced the numerical simulation principle of FE-MSE method, with frequency-dependent mechanical behaviors of viscoelastic polyurea considered. How key geometric parameters affected natural frequencies and damping loss factors of LASCOR sandwich panels with PML face sheets were systematically investigated in Section 4. The superiority of such novel panels over monolithic panels having equal mass was also highlighted. Section 5 analyzed the fidelity of surrogate model on damping loss factor, and proposed a series of optimization problems to explore superior performance of structural stiffness and vibration attenuation.

2. Review of experiments

In a previous study [24], LASCOR sandwich panels with PML face sheets were proposed and fabricated, and their effectiveness for passive vibration suppression was systematically estimated. For completeness of the current study, relevant fabrication process and experimental results were briefly reviewed below.

2.1. Experimental procedure

The fabrication details mainly consisted of four steps, as illustrated in Fig. 1. Trapezoidal corrugated cores were fabricated firstly using the stamping process; for enhanced bonding between the corrugated core and the face sheets, a corrugation platform was introduced as shown in Fig. 1a. Next, the face sheets and corrugated core were linked together in sequence via laser welding. Compared with vacuum brazing [4], laser welding provided a more convenient and efficient assembling of large-scale sandwich components for engineering applications. The as-fabricated bare corrugated sandwich panel was subsequently placed into a polymer mould. Uncured polyurea (Qtech-413, Qingdao Shamu Advanced Material Co., Ltd.) was sufficiently stirred, and then poured onto the surface of the sandwich panel promptly. Immediately after the uncured polyurea uniformly covered the whole surface, an extra thin metal plate was quickly placed on top of the polyurea layer. After two weeks of curing at room temperature, LASCOR sandwich panels with three different types of face sheet were fabricated, and their geometrical configuration were illustrated in Fig. 2. In comparison with the conventional sandwich panel with monolithic metal face sheets (i.e., without polyurea coating; Fig. 2a), the proposed LASCOR sandwich panels have either PML-A (metal/polyurea/metal laminate) or PML-B (polyurea/metal laminate) face sheets (Fig. 2b–d).

The effectiveness of using PML face sheets for passive vibration suppression of all-metallic corrugated sandwich panels were measured via modal vibration tests, as depicted in Fig. 3. Fixed by two rubber ropes, the specimen was suspended in a steel bracket to simulate free-edge boundary condition. The modal testing setup mainly consisted of an impact hammer (Model 086C03, PCB Piezotronics, Inc.), an accelerometer (Model 333B32, PCB Piezotronics, Inc.), and a monitoring laptop linked with a dynamic analyzer (DongHua Modal Analysis). The sensitivity, measurement range, and weight of the impact hammer are 2.25 mV N^{-1} , $\pm 2224 \text{ N pk}$ and 0.16 kg , respectively. Similarly, these parameters of the accelerometer are $10.2 \text{ mV m}^{-1} \text{ s}^2$, $\pm 490 \text{ m s}^{-2} \text{ pk}$ and 0.004 kg , respectively. To reduce the experimental error, the weight ratio of the accelerometer and specimen

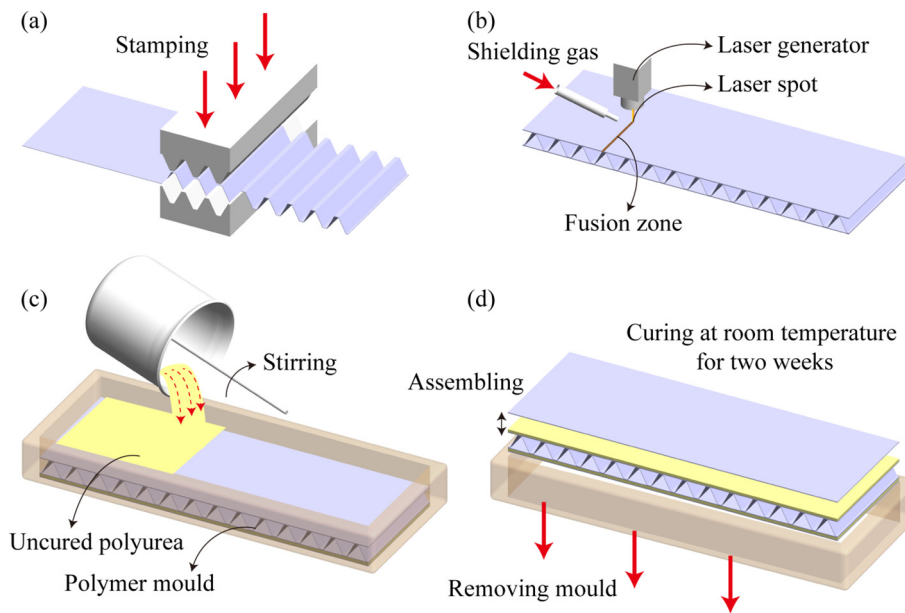


Fig. 1. Fabrication process of laser-welded corrugated-core (LASCOR) sandwich panel with polyurea-metal laminates (PMLs) as skins: (a) forming corrugated core, (b) laser welding, (c) forming polyurea layer, and (d) assembling and curing.

should be as small as possible. With the method of point-by-point excitation adopted, both force and acceleration signals were collected and transferred to the dynamic analyzer, and then processed in the monitoring laptop. Therefore, frequency/time response spectrums, natural frequencies, mode shapes and damping loss factors of each specimen could be obtained. Detailed theoretical analysis of the modal testing technique was summarized in our previous study [32].

2.2. Experimental results

Time response spectrums of sandwich panels with PML face sheets were compared with those without PML face sheets, and the corresponding decay time was preliminarily utilized to assess the effectiveness of passive vibration suppression. To facilitate visual comparison, the acceleration signals were normalized by their respective maximum acceleration values. As shown in Fig. 4a, under the same excitation force, specimen S-4 with polyurea coating exhibited a more effective capacity to passively suppress the acceleration signal compared with S-1 without polyurea coating. That is, PML face sheets could dissipate vibration energy via sufficient viscoelastic deformation of the embedded polyurea layers. Further, the first three damping loss factors were measured to quantitatively evaluate the intrinsic structural behavior associated with vibration suppression. As shown in Fig. 4b, the panels with PML skins achieved remarkable enhancement in damping loss factors. In particular, specimen S-6 with uniform distribution of polyurea on two skins possessed the highest damping loss factors, more than 10 times larger than those of S-1. Physical mechanisms underlying such enhancement were discussed in detail in our previous work [24]. Moreover, the first three natural frequencies of sandwich panels with PML face sheets were found to decrease by approximately 10 ~ 20%, depending on the variation of structural flexural stiffness and total weight.

3. Numerical modeling

3.1. FE-MSE method

In order to predict the vibration damping features of LASCOR sandwich panels with PML face sheets, a combined finite element-modal

strain energy (FE-MSE) method was employed based on the commercial FE code ABAQUS/CAE 2016.

Firstly, we construct the FE models of LASCOR sandwich panels with PML face sheets with their detailed geometric parameters illustrated in Fig. 2. Both the face sheets and the corrugated core were modeled using the linear 4-node shell element S4R, while the polyurea layers were meshed using the linear 8-node brick element C3D8R. Upon applying the tie constraints, all the components of the sandwich panel were perfectly bonded together. Without any boundary conditions applied, the FE models were expected to simulate the actual edge-free boundary conditions in our modal tests (Fig. 3). The linear perturbation step of frequency analysis with Lanczos eigensolver was conducted to obtain the first three modal characteristics, such as the natural frequencies and mode shapes. In this step, both the parent metal (304 stainless steel) and the polyurea material were considered as linear elastic materials. Input parameters of the former were obtained from our previous work [24]: mass density $\rho_s = 7930 \text{ kg m}^{-3}$, Young's modulus $E_s = 200 \text{ GPa}$ and damping loss factor $\eta_s = 0.006$. As to the viscoelastic polyurea with a mass density of $\rho_p = 1000 \text{ kg m}^{-3}$, its complex Young's modulus E_p was expressed as:

$$E_p = E'_p + iE''_p = E'_p(1 + i\eta_p) \quad (1)$$

$$\eta_p = \frac{E''_p}{E'_p} \quad (2)$$

where η_p represents the damping loss factor of polyurea. The real part of the complex modulus (storage modulus), E'_p , should be employed in the FE model [33]. However, both E'_p and η_p exhibited frequency dependency in the testing range, as shown in Fig. 5b-c. Thus, to improve the prediction accuracy, the frequency sensitivity of polyurea was taken into consideration in the current study. The detailed simulation algorithm of the FE-MSE method was summarized in Fig. 5a, which was similar to previous studies [34,35]. Note that, the frequency corresponding to the initial storage modulus E'_{p0} was set as 1 Hz. Fig. 5b-c presented the storage modulus and damping loss factors measured in 1, 10, 50, 100, 150 Hz via dynamic thermomechanical analysis (DMA) tests. The more detailed DMA observations of the polyurea

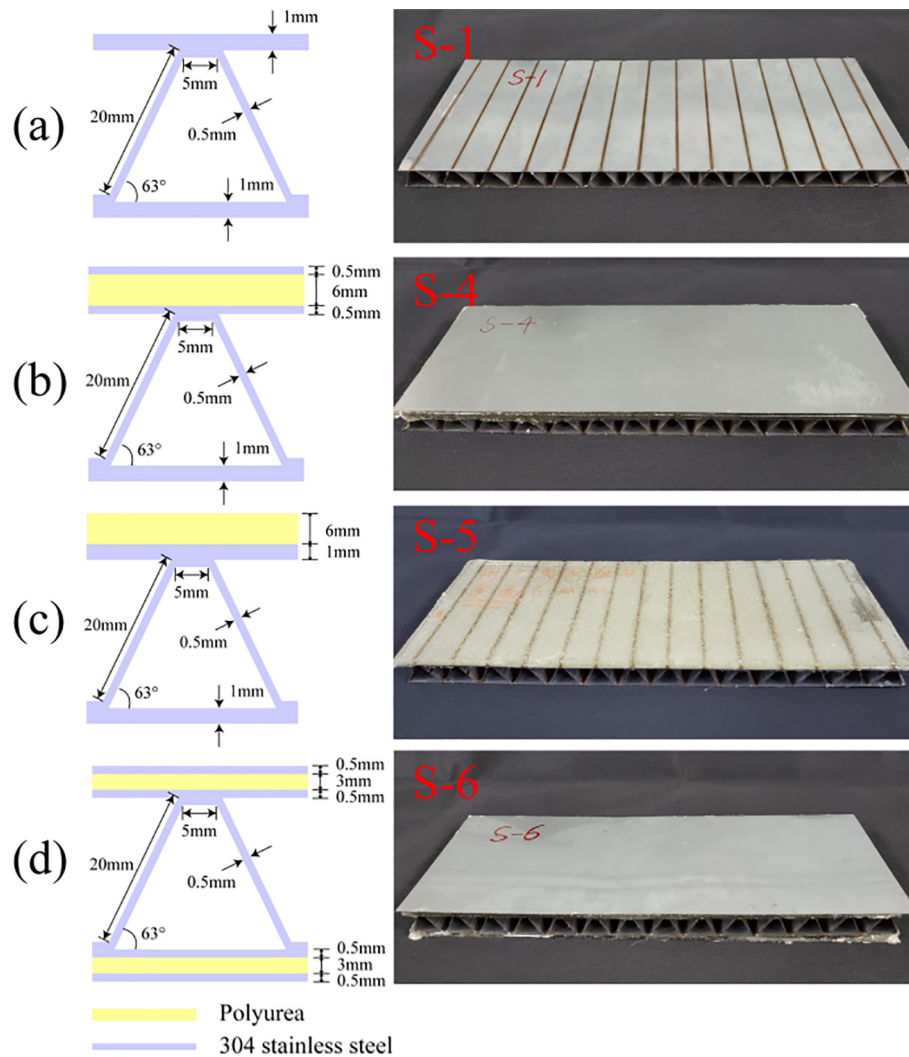


Fig. 2. Geometric illustration of as-fabricated sandwich panels: (a) specimen S-1 without polyurea coating, (b) specimen S-4 with single PML-A face sheet, (c) specimen S-5 with single PML-B face sheet, and (d) specimen S-6 with double PML-A face sheets.

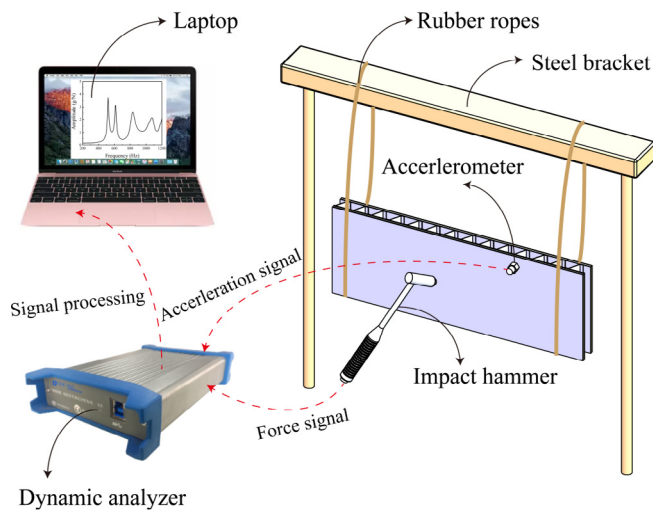


Fig. 3. Modal testing set-up.

elastomer have already been present in our recent work [24]. Nevertheless, the concerned first three natural frequencies might exceed 150 Hz. Thus, in order to expand the frequency range to 150–1200 Hz, both the

Havriliak-Negami (H-N) model [36] and the Kelvin-Voigt (K-V) model [37] were introduced to fit the DMA testing data through Levenberg-Marquardt algorithm, respectively. The two classical theoretical models could be expressed as:

$$E_p'(f) = c_2 + \frac{(c_1 - c_2) \cos \left(c_4 \tan^{-1} \left(\frac{(2\pi f)^{c_3} \sin(\frac{c_3\pi}{2})}{1 + (2\pi f)^{c_3} \cos(\frac{c_3\pi}{2})} \right) \right)}{\left(1 + 2(2\pi f)^{c_3} \cos(\frac{c_3\pi}{2}) + (2\pi f)^{2c_3} \right)^{\frac{c_4}{2}}} \quad (3)$$

$$\eta_p(f) = \frac{d_1 (2\pi f)^{d_3} \sin(\frac{d_3\pi}{2})}{d_1 (2\pi f)^{d_3} \cos(\frac{d_3\pi}{2}) + d_2} \quad (4)$$

where f is the testing frequency, $c_1 \sim c_4$ are the undetermined coefficients of the H-N model, and $d_1 \sim d_3$ are the undetermined coefficients of the K-V model. The detailed fitting results were also marked in Fig. 5-b-c.

As shown in Fig. 5a, we could obtain a valid natural frequency upon the iterative FE simulations. Then, the corresponding damping loss factor was further estimated by means of the modal strain energy (MSE) method introduced by Johnson and Kienholz [33]. Compared with directly solving the complex eigenvalues and eigenvectors, the MSE method only needs to calculate the undamped modes; corresponding energy distributions can be obtained to determine the

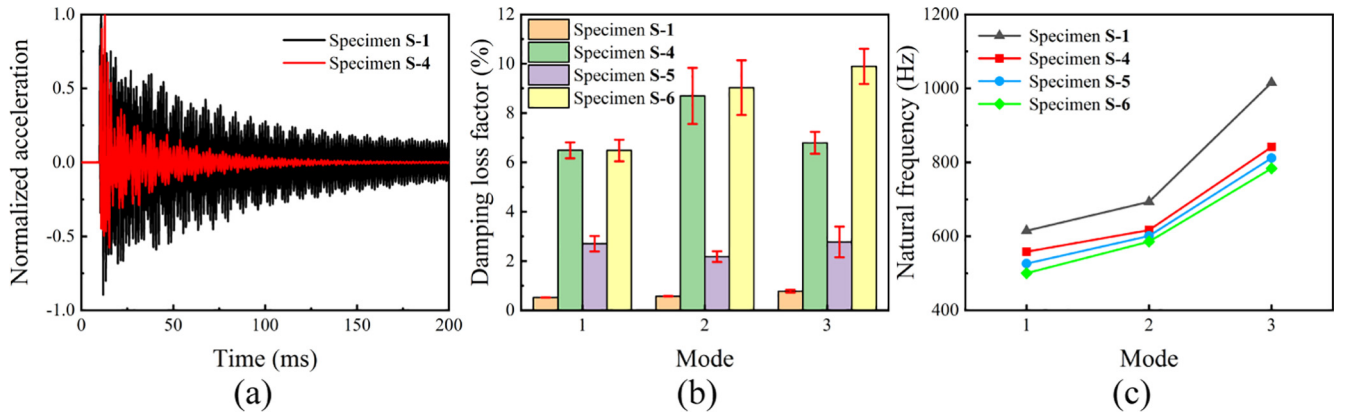


Fig. 4. Experimental results of LASCOR sandwich panels with and without PML face sheets: (a) time response spectrums, (b) damping loss factors, (c) natural frequencies.

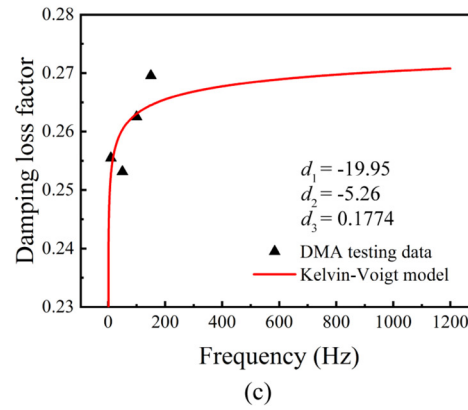
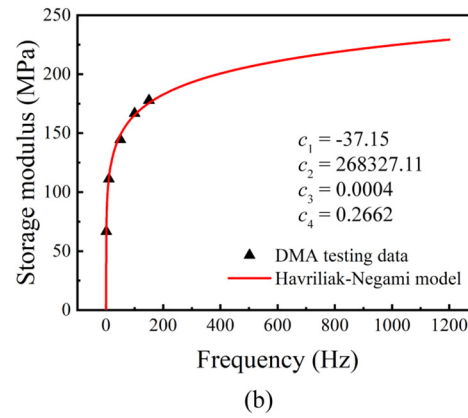
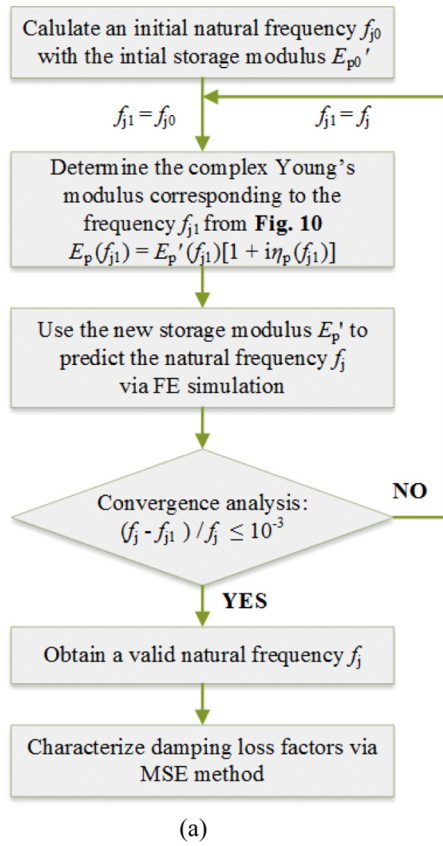


Fig. 5. (a) The simulation algorithm of the FE-MSE method, and the fitting curves of (b) storage modulus and (c) damping loss factor of polyurea as functions of testing frequency (0–1200 Hz) at room temperature.

damping characteristics. The basic assumption of the MSE method is that the damped and undamped mode shapes of a structure are identical [33], so that the damping loss factor corresponding to the r^{th} mode can be estimated as:

$$\eta^{(r)} = \frac{\Delta U^{(r)}}{U^{(r)}} = \frac{\sum_{i=1}^m \eta_s^{(r)} u_{s,i}^{(r)} + \sum_{j=1}^n \eta_p^{(r)} u_{p,j}^{(r)}}{\sum_{i=1}^m u_{s,i}^{(r)} + \sum_{j=1}^n u_{p,j}^{(r)}} \quad (5)$$

where the superscript (r) represents the r^{th} mode, $\Delta U^{(r)}$, $U^{(r)}$ are the total stored strain energy and dissipated strain energy, respectively. $u_{s,i}^{(r)}$ is the stored energy of element i in the metallic sandwich component, $u_{p,j}^{(r)}$ is the stored energy of element j in the polyurea layer, while

$\eta_s^{(r)}$ and $\eta_p^{(r)}$ are the material loss factors of 304 stainless steel and polyurea material corresponding to the r^{th} natural frequency. Further, $u_{s,i}^{(r)}$ and $u_{p,j}^{(r)}$ can be written as:

$$u_{s,i}^{(r)} = \frac{1}{2} \sum \int_{V_{s,i}} \sigma_{kl} \epsilon_{kl} dV_{s,i} (k, l = x, y, z) \quad (6)$$

$$u_{p,j}^{(r)} = \frac{1}{2} \sum \int_{V_{p,j}} \sigma_{kl} \epsilon_{kl} dV_{p,j} (k, l = x, y, z) \quad (7)$$

where σ_{kl} and ϵ_{kl} ($k, l = x, y, z$) are the stress and strain component, respectively. $V_{s,i}$ and $V_{p,j}$ are separately the volume of element i in

the metallic sandwich component and the volume of element j in the polyurea layer. All of these stress and strain information were output from the final step of the iterative FE simulations. The global coordinate system (x, y, z) attributes to the finite element model, as shown later in Fig. 7c.

3.2. Mesh convergence

We carried out a mesh convergence study using different mesh sizes (1.5, 2, 3, 4, 5 mm) in order to determine an optimal mesh size for FE simulations. Specifically, 20 processors (Intel Xeon Gold 6134, 3.20 GHz) were employed to construct a series of parallel computation. The first three natural frequencies of the undamped sandwich panel (i.e., without polyurea coating) thus calculated were displayed in Fig. 6a. These natural frequencies appeared to converge as the mesh size was reduced to be less than 2 mm, and the difference in simulation results obtained with mesh sizes of 1.5 and 2 mm was not obvious. However, the FE model with 1.5 mm mesh size took 60% longer to obtain the first three natural frequencies, as shown in Fig. 6b. Thus, for balanced computational cost and numerical accuracy, the overall mesh size of 2 mm was adopted in all subsequent numerical simulations.

3.3. Validation study

To validate the proposed FE-MSE method, the first natural frequencies, damping loss factors, and mode shapes obtained from modal tests were compared with numerical simulation results. As shown in Fig. 7a-b, the current simulations provided a reasonable prediction on the vibration and damping characteristics of LASCOR sandwich panels with PML face sheets. As an example, the first mode shapes of specimen S-6 consisting of bending and torsional modes were compared in Fig. 7c. The mode shapes obtained from modal tests agreed well with those calculated numerically. However, some discrepancies did exist, especially in the third natural frequencies. According to our previous analysis [32], the natural frequencies were sensitive to the boundary condition, the laser welding defects, the corrugation forming defects, and the like. On the other hand, the structural damping characteristics were associated with the fabrication process, the boundary condition, and the testing set-up [22,38]. For instance, the rubber ropes might cause an extra damping effect but this effect was ignored in the current simulation. In addition, fabrication defects of laser welding joints and polyurea layers were not taken into consideration. Nonetheless, although it was quite difficult to eliminate the above-mentioned error sources completely, the present numerical simulations were accurate enough and could be exploited to provide a parametric study, as illustrated in the section that follows.

4. Parametric study

In this section, a comprehensive parametric investigation on the vibration damping characteristics of LASCOR sandwich panels with PML face sheets was carried out to determine the optimization variables. From the experimental results (Fig. 4), specimen S-6 with two symmetric PML-A face sheets exhibited the best performance in passive vibration suppression. As the corresponding damping enhancement mechanisms had already been explored [24], the present parametric study and further multi-objective optimization focused upon this panel configuration.

As shown in Fig. 8, the LASCOR sandwich panel had two identical PML-A face sheets, each consisting of a base metal layer, a polyurea layer and a constrained metal layer. The relative density of the corrugated core, $\bar{\rho}$, was given by:

$$\bar{\rho} = \frac{t_c(t_p + l_c)}{(l_p + l_c \cos\theta)(t_c + l_c \sin\theta)} \quad (8)$$

Key geometric parameters of the sandwich panel included panel length L , panel width W , base metal layer thickness t_{fb} , constrained metal layer thickness t_{fc} , polyurea layer thickness t_p , corrugated core thickness t_c , height H_c , corrugation member length l_c , inclination angle θ , and plateau length l_p . The sandwich panel was assumed to contain 14 unit cells along the x -axis, and their width along the y -axis was fixed at $W = 140$ mm. Besides, the corrugation plateau was fixed at $l_p = 5$ mm to ensure good bonding between PML face sheets and corrugation core. Under these circumstances, the influences of six independent geometric parameters (i.e., t_{fb} , t_{fc} , t_p , t_c , l_c , θ) were systematically discussed, with their initial designs set as $t_{fb} = 0.5$ mm, $t_{fc} = 0.5$ mm, $t_p = 3$ mm, $t_c = 0.5$ mm, $l_c = 20$ mm and $\theta = 63^\circ$.

4.1. Natural frequencies

Fig. 9 presented the different sensitivities of the first three natural frequencies to the six key geometric parameters: t_{fb} , t_{fc} , t_p , t_c , l_c , and θ . With the material properties fixed, each of the geometric parameters varied uniformly. As depicted in Fig. 9a-c, the first three natural frequencies were positively correlated with the variation of PML face sheets, especially for base metal layer thickness t_{fb} (Fig. 9a). By contrast, the positive effects of the thickness of polyurea and constrained metal layers were small, even not obvious. Similarly, as shown in Fig. 9d-f, variation of the corrugated core also significantly affected the first natural three frequencies, although different trends were observed. To be specific, the natural frequencies were positively proportional to t_c , θ , but negatively to l_c . The factors accounting for such different trends were discussed in our previous work [32].

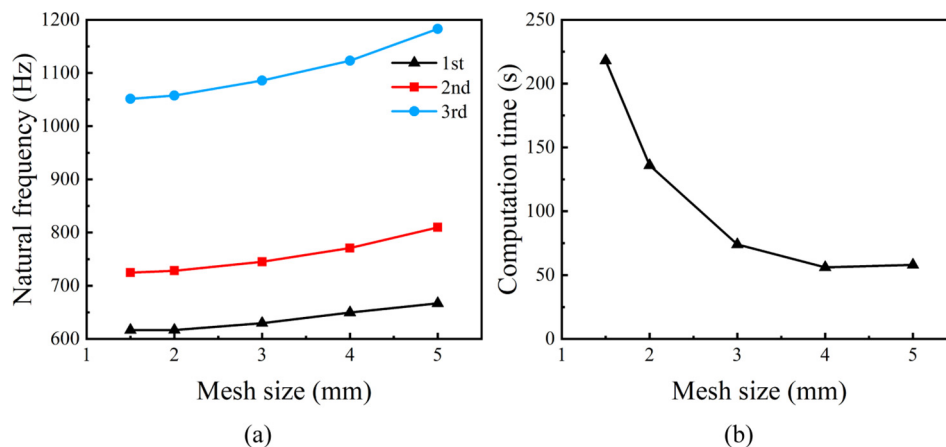


Fig. 6. Influence of mesh size on (a) the first three natural frequencies of sandwich panel without polyurea coating and (b) the corresponding computation time.

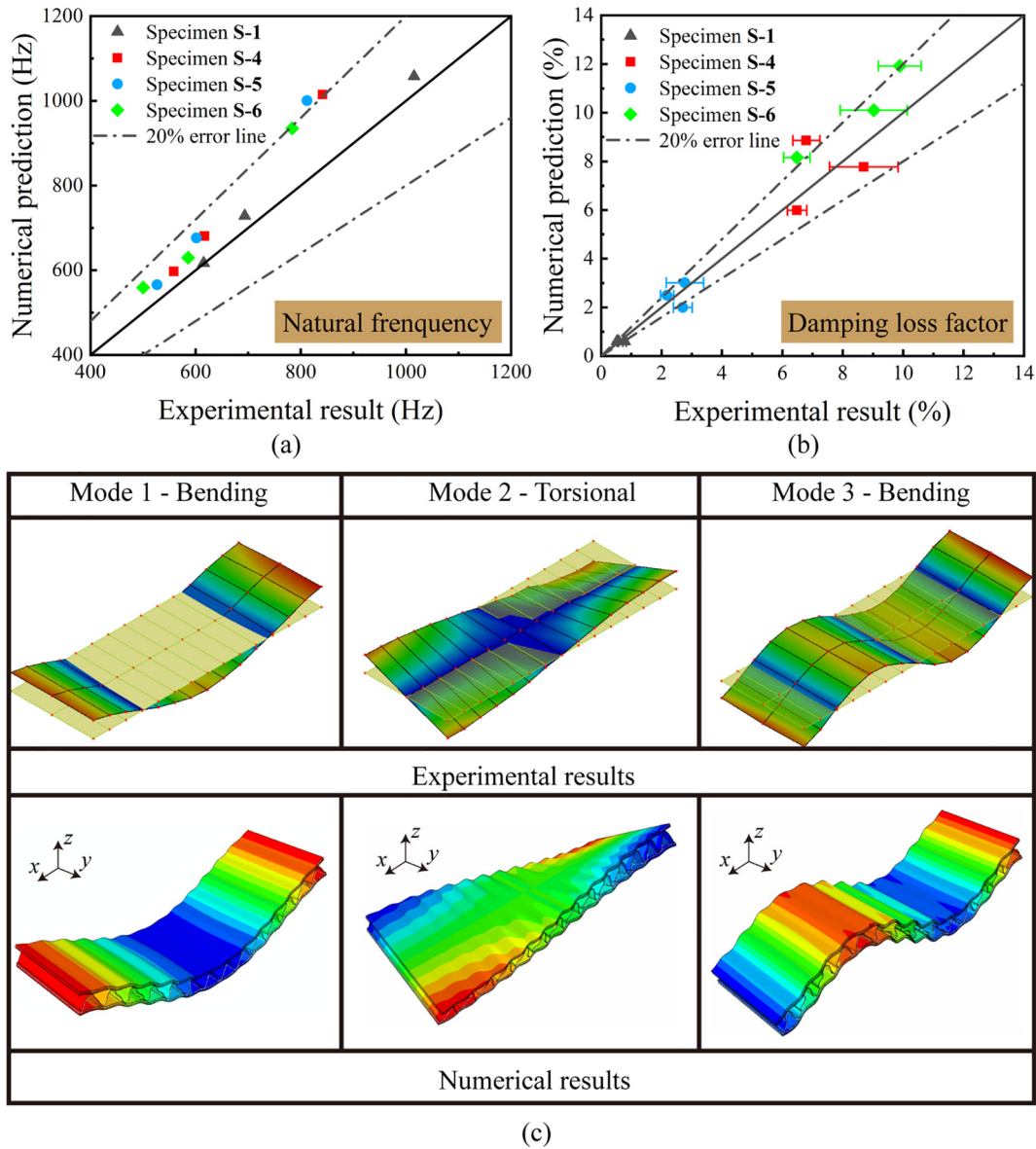


Fig. 7. Validation analysis of the proposed FE-MSE method: (a) natural frequencies, (b) damping loss factors, and (c) mode shapes.

In a nutshell, most theoretical models substantiated a common belief that the natural frequencies of a sandwich structure were determined by its flexural stiffness, transverse shear stiffness and structural weight [39]. Based on the first shear deformation theory, Timoshenko [40] proposed an analytical solution to the first natural frequency of a prismatic beam with simple supported ends, as:

$$p_m = \frac{\pi^2}{L_w^2} \sqrt{\frac{EIg}{\rho\Omega}} \left[1 - \frac{1}{2} \frac{\pi^2 I}{L^2 \Omega} \left(1 + \frac{E}{\lambda\Lambda} \right) \right] \quad (9)$$

where Λ is the modulus of transverse shear stiffness, λ is a constant relying upon the shape of beam cross section, L_w is the length of a wave, EI is the flexural stiffness of the prismatic bar, Ω is the area of the cross section, and ρ/g is the density of the base material. For a LASCOR sandwich panel, its flexural stiffness and shear stiffness were mainly contributed by the PML face sheets and the corrugated core, respectively. Therefore, based on Eq. (9), enlarging the PML skin thickness increased the flexural stiffness, and accordingly led to the increase of natural frequencies. Likewise, varying the corrugated core also affected the shear stiffness, and further changed the natural frequencies.

To highlight the superiority of a LACOR sandwich panel over its monolithic counterpart, a dimensionless frequency parameter was proposed as f/f_0 , where f and f_0 were the natural frequencies of the sandwich panel and the corresponding monolithic panel having identical length, width, weight and boundary conditions, respectively. Similar approach was adopted in our previous studies [32,41]. The thickness of the monolithic panel, h_m , was:

$$h_m = \bar{\rho} H_c + 2t_{fb} + 2t_{fc} + 2t_{fc} + \frac{2\rho_p t_p}{\rho_s} \quad (10)$$

where $H_c = (l_c \sin\theta + t_c)$ is the thickness of corrugated core. Fig. 10a–c displayed the numerically calculated influences of geometric parameters (t_{fb} , t_{fc} , t_p , t_c , l_c , θ) on the dimensionless frequencies. The dimensionless frequencies decreased as the thickness of PML face sheets was increased, indicating that the superiority of sandwich panels over solid ones peaked under the condition of low mass density. The same trend of t_c was also observed in Fig. 10d. Apart from the results of Fig. 10a–d, two different variation trends with l_c and θ were observed in Fig. 10e–f. Note that, the first dimensionless frequency was higher

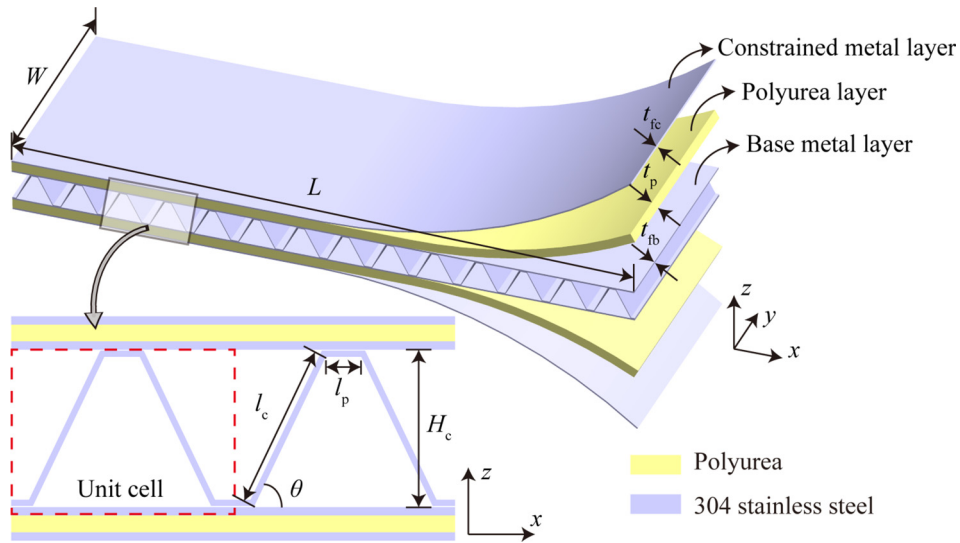


Fig. 8. Geometric illustration of a LASCOR sandwich panel with two symmetric PML-A face sheets.

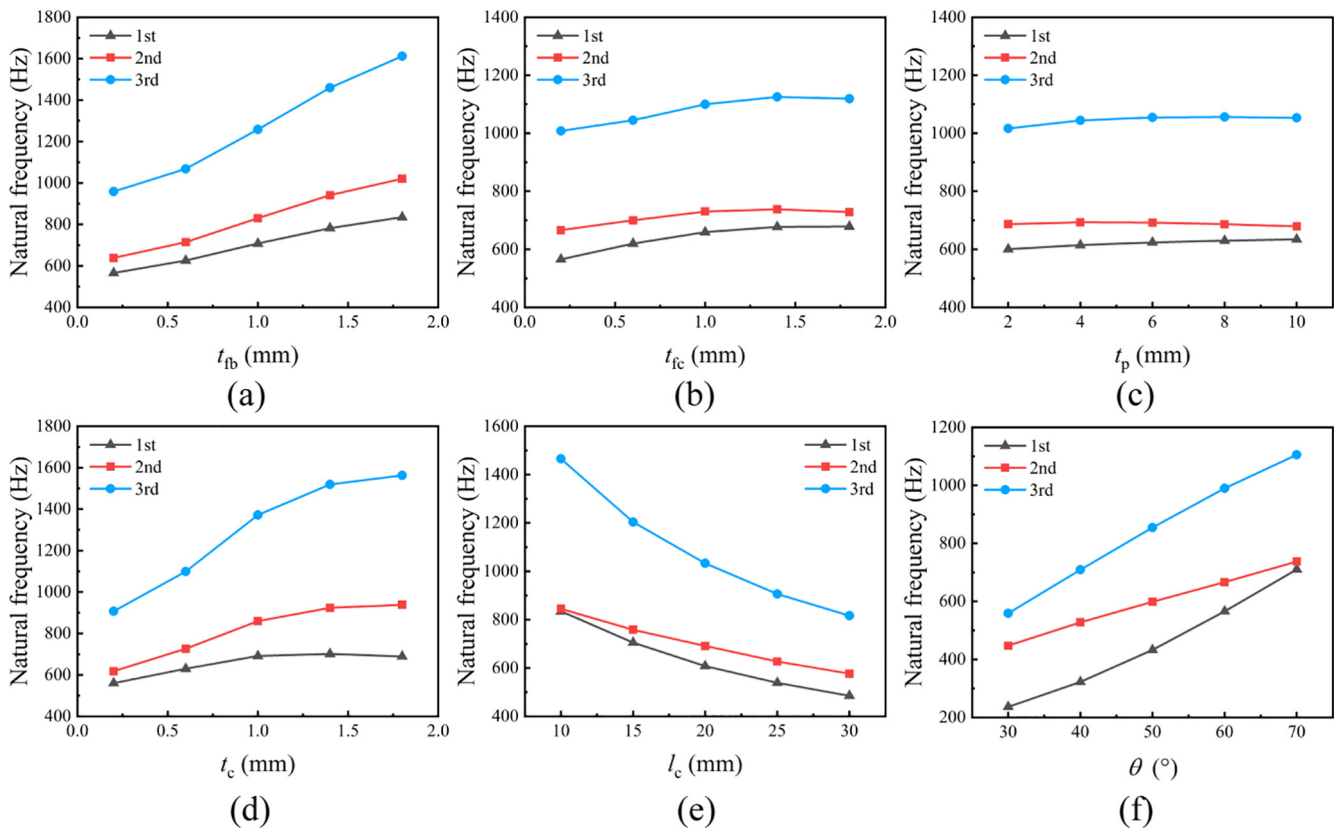


Fig. 9. Sensitivity of the first three natural frequencies to key geometric parameters: (a) base metal layer thickness t_{fb} , (b) constrained metal layer thickness t_{fc} , (c) polyurea layer thickness t_p , (d) corrugated core thickness t_c , (e) corrugation member length l_c and (f) inclination angle θ .

than the other two, demonstrating that the superiority of sandwich panels was more obvious at low frequencies.

4.2. Damping loss factors

Fig. 11 presented the different sensitivities of the first three damping loss factors to key geometric parameters (t_{fb} , t_{fc} , t_p , t_c , l_c , θ). Again, with the material properties fixed, each geometric parameter was varied uniformly. As shown in Fig. 11a–c, the damping loss factors were

positively proportional to t_{fc} , t_p , but negatively to t_{fb} . That is, for enhanced passive vibration attenuation, the constrained metal and polyurea layers should have large thicknesses while keeping the base metal layer relatively thin. Similar results were discussed in a NASA report concerning the design of CLD (constrained layer damping) structures [42]. Based on the theoretical basis of the MSE method (i.e., Eqs. (5)–(7)), the other three geometric parameters mainly affected the modal strain energy proportion of each sandwich component, thus further changing the damping loss factors (Fig. 12d–f).

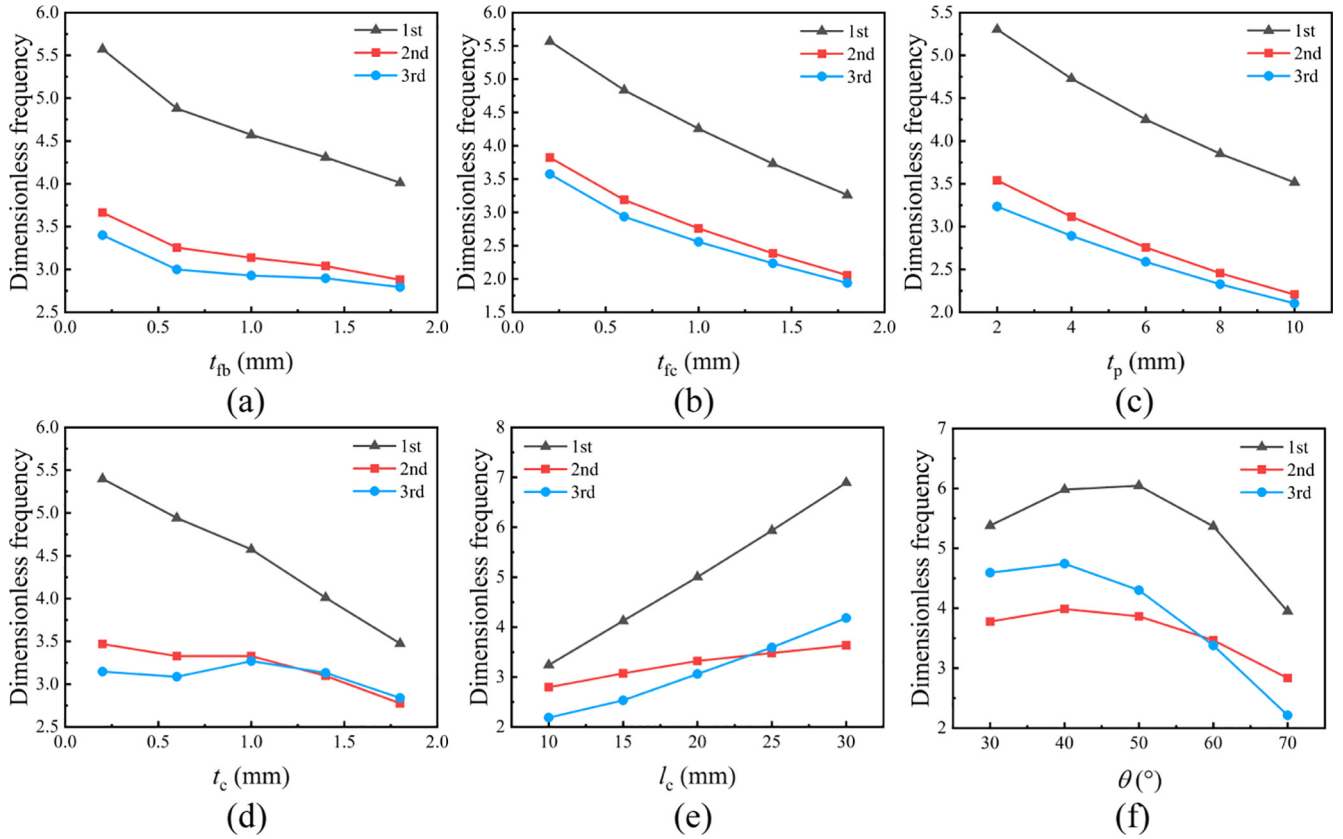


Fig. 10. Sensitivity of the first three dimensionless frequencies to key geometric parameters: (a) base metal layer thickness t_{fb} , (b) constrained metal layer thickness t_{fc} , (c) polyurea layer thickness t_p , (d) corrugated core thickness t_c , (e) corrugation member length l_c and (f) inclination angle θ .

Similar to natural frequencies, to further highlight the superiority of LACOR sandwich panels, a dimensionless loss factor parameter ζ/ζ_0 was introduced, ζ and ζ_0 being the damping loss factors of the sandwich panel and the monolithic panel having the same length, width, weight and boundary conditions. Herein, the damping loss factor of the monolithic panel was set as 0.006, similar to that used in numerical simulations. As shown in Fig. 12, the present sandwich panel significantly outperformed its monolithic counterpart on passive vibration attenuation, quantitatively by as large as 20 times. In a word, the results of Figs. 9 and 11 demonstrated that geometric parameters affected the natural frequencies and damping loss factors in different manners, especially the PML parameters. It follows that the optimal geometric parameters of LACOR sandwich panels with PML face sheets need to be explored for combined structural stiffness, vibration damping and structural weight.

5. Optimal design

An optimum structure is expected to combine high structural stiffness, high capacity of passive vibration and lightweight. To this end, the optimal design of LASCOR sandwich panels with two symmetric PML-A skins (Fig. 8) for combined vibration damping and structural stiffness were carried out in this section. Based on the commercially available mathematics software MATLAB R2019b, the flow chart of the current optimization was presented in Fig. 13.

5.1. Definition of optimization problem

According to the analysis detailed in Section 4, to demonstrate the optimization approach, three independent geometric parameters (t_{fb} , t_{fc} , t_p) were identified as the design variables to generate a design

space, which were constrained by $0.2 \text{ mm} < t_{fb} < 1.8 \text{ mm}$, $0.2 \text{ mm} < t_{fc} < 1.8 \text{ mm}$, and $1 \text{ mm} < t_p < 10 \text{ mm}$. For simplicity, the other three geometric parameters were fixed at $t_c = 0.5 \text{ mm}$, $l_c = 20 \text{ mm}$ and $\theta = 63^\circ$. Note that, the length and width of the sandwich panel were $L = 28(l_p + l_c \cos\theta)$ and $W = 140 \text{ mm}$. Then, two important parameters were chosen as design objectives to evaluate the capacity of the sandwich panel for simultaneous vibration attenuation and structural stiffness, i.e., the first damping loss factor η and the sum of transverse and longitudinal flexural stiffness D . The latter was written as:

$$D = D_x + D_y \quad (11)$$

$$D_x = \frac{1}{12}L \left(\begin{aligned} &8E_s \left(\left(\frac{1}{2}(l_c \sin\theta + t_c) + t_{fb} + t_{fc} + t_p \right)^3 - \left(\frac{1}{2}(l_c \sin\theta + t_c) + t_{fb} + t_p \right)^3 \right) \\ &+ 8E_p \left(\left(\frac{1}{2}(l_c \sin\theta + t_c) + t_{fb} + t_p \right)^3 - \frac{1}{8}(l_c \sin\theta + t_c + 2t_{fb})^3 \right) \\ &+ E_s \left((l_c \sin\theta + t_c + 2t_{fb})^3 - (l_c \sin\theta + t_c)^3 \right) + C_{22}^H (l_c \sin\theta + t_c)^3 \end{aligned} \right) \quad (12)$$

$$D_y = \frac{1}{12}W \left(\begin{aligned} &8E_s \left(\left(\frac{1}{2}(l_c \sin\theta + t_c) + t_{fb} + t_{fc} + t_p \right)^3 - \left(\frac{1}{2}(l_c \sin\theta + t_c) + t_{fb} + t_p \right)^3 \right) \\ &+ 8E_p \left(\left(\frac{1}{2}(l_c \sin\theta + t_c) + t_{fb} + t_p \right)^3 - \frac{1}{8}(l_c \sin\theta + t_c + 2t_{fb})^3 \right) \\ &+ E_s \left((l_c \sin\theta + t_c + 2t_{fb})^3 - (l_c \sin\theta + t_c)^3 \right) + C_{11}^H (l_c \sin\theta + t_c)^3 \end{aligned} \right) \quad (13)$$

where D_x and D_y are transverse and longitudinal flexural stiffness of the sandwich panel, while C_{11}^H and C_{22}^H are two in-plane effective elastic constants of the corrugated core:

$$C_{11}^H = \frac{E_s}{(1 - \nu_s^2)} \left(\frac{t_c}{l_c} \right) \frac{\cos^3\theta}{\sin\theta} + \frac{E_s}{(1 - \nu_s^2)} \left(\frac{t_c}{l_c} \right)^3 \sin\theta \cos\theta \quad (14)$$

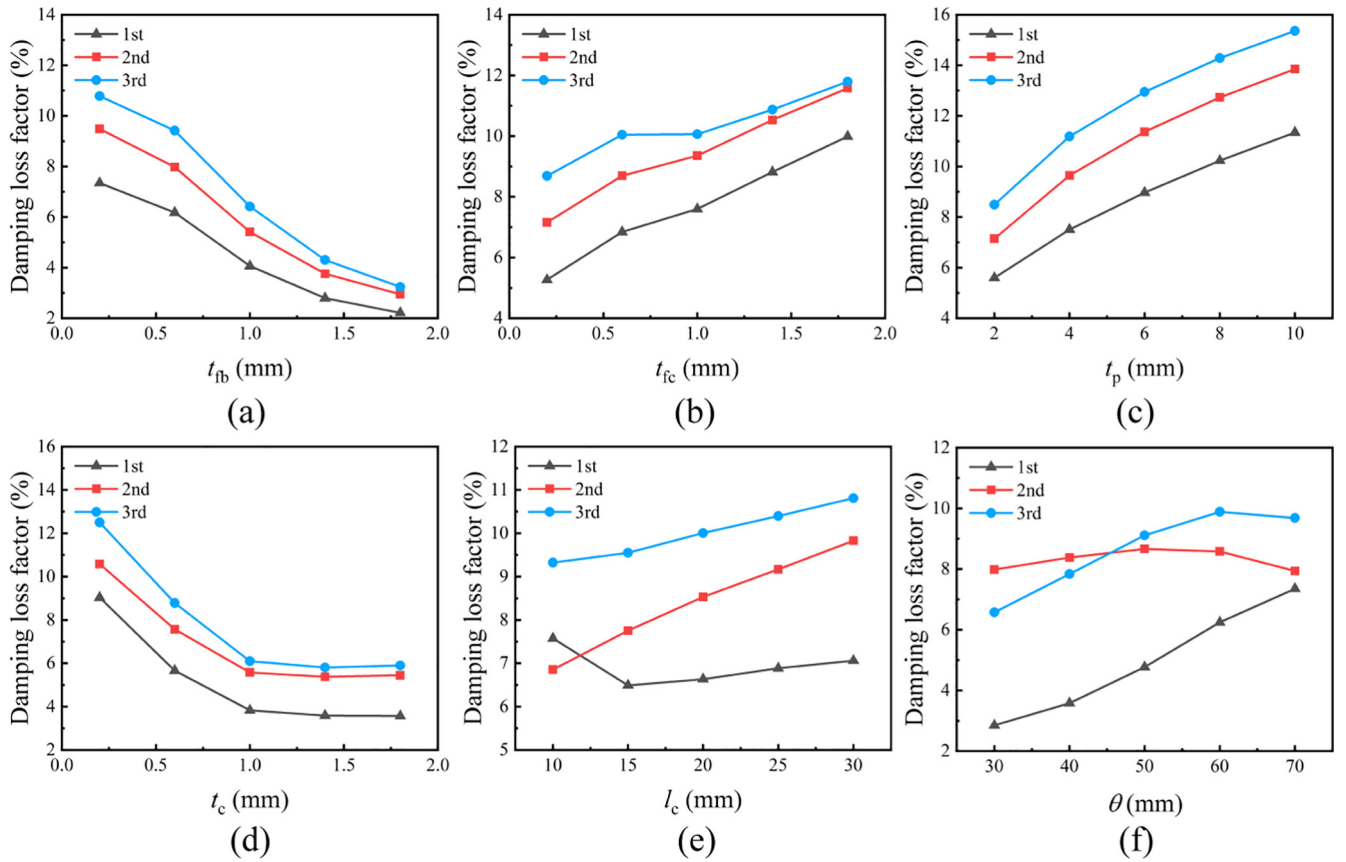


Fig. 11. Sensitivity of the first three damping loss factors to key geometric parameters: (a) base metal layer thickness t_{fb} , (b) constrained metal layer thickness t_{fc} , (c) polyurea layer thickness t_p , (d) corrugated core thickness t_c , (e) corrugation member length l_c and (f) inclination angle θ .

$$C_{22}^H = \bar{\rho} \frac{E_s}{(1 - \nu_s^2)} \quad (15)$$

Note that, the corrugated core was treated as an equivalent orthotropic core, and its effective elastic stiffness matrix was derived using the homogenization theory (more details could be found in [43,44]). The total weight M of the sandwich panel was expressed as:

$$M = LW[(4t_f + \bar{\rho}(l_c \sin\theta + t_c))\rho_s + 2t_p\rho_p] \quad (16)$$

where $\bar{\rho}$ is the relative density of corrugated core. However, obtaining an analytical solution of the other design objective (i.e., first damping loss factor η) was difficult, due to its highly nonlinear relationship with the design variables. A surrogate modeling technique was therefore employed to evaluate η in an approximate way, as detailed in Section 5.2.

Under these circumstances, three optimization problems were defined, including one single-objective problem and two multi-objective ones, as shown in Table 1. To highlight the importance of the present optimization schemes, specimen S-6 was selected as the optimization target, with a preliminary design of $D_0 = 29467 \text{ Pa m}^4$, $\eta_0 = 6.634\%$ and $M_0 = 1.59 \text{ kg}$.

5.2. Surrogate model

5.2.1. Model description

Generally speaking, the vibration damping characteristics of the LASCOR sandwich panel with PML face sheets is complicated, due to nonlinear frequency-dependent energy dissipation of viscoelastic polyurea. Surrogate modeling was thus implemented into the optimization task. In the current study, the feasibility of four surrogate models was systematically analyzed. Table 2 listed relevant parameters and

functions of the four models. The design space was sampled and 60 sampling points were generated using the Optimal Latin Hypercube (OLH) method, as listed in Table 3. This type of DoE (Design of Experiment) technique spreads sampling points evenly to capture higher order effects, and the number of sampling points should be greater than that of design variables [45].

5.2.2. Surrogate accuracy

Following the principle of cross-validation error analysis [50], surrogate accuracy was identified. That is, a certain number of validation points were removed from the sampling point set, one at a time. For each of the removed points, the approximation coefficients were recalculated, and both the actual (FE-MSE) and predicted (surrogate model) results were compared. The currently removed point was then put back into the sampling point set, and the next point was removed. Note that, 30 validation points were selected randomly from the sampling set in this work. Relative error of the surrogate models was evaluated using R-square (R^2), Root-Mean-Square-Error (RMSE), Maximum-Absolute-Percentage-Error (MAPE), as follows:

$$R^2 = 1 - \frac{\sum_{i=1}^{M_v} (y_i - \hat{y}_i)^2}{\sum_{i=1}^{M_v} (y_i - \bar{y}_i)^2} \quad (17)$$

$$\text{RMSE} = \sqrt{\frac{1}{M_v} \sum_{i=1}^{M_v} (\hat{y}_i - y_i)^2} \quad (18)$$

$$\text{MAPE} = \max\left(\frac{|\hat{y}_i - y_i|}{y_i}\right) \quad (19)$$

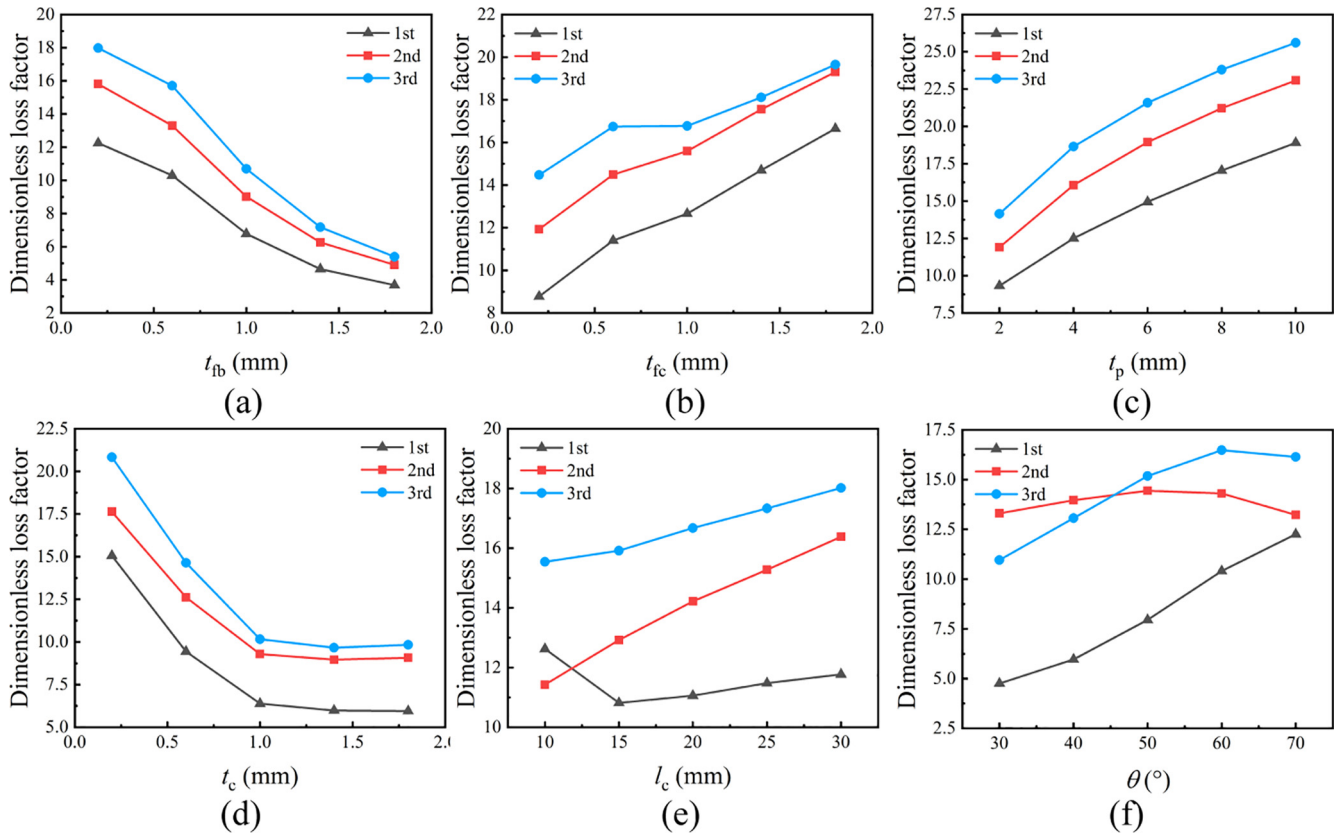


Fig. 12. Sensitivity of the first three dimensionless loss factors to key geometric parameters: (a) base metal layer thickness t_b , (b) constrained metal layer thickness t_{fc} , (c) polyurea layer thickness t_p , (d) corrugated core thickness t_c , (e) corrugation member length l_c and (f) inclination angle θ .

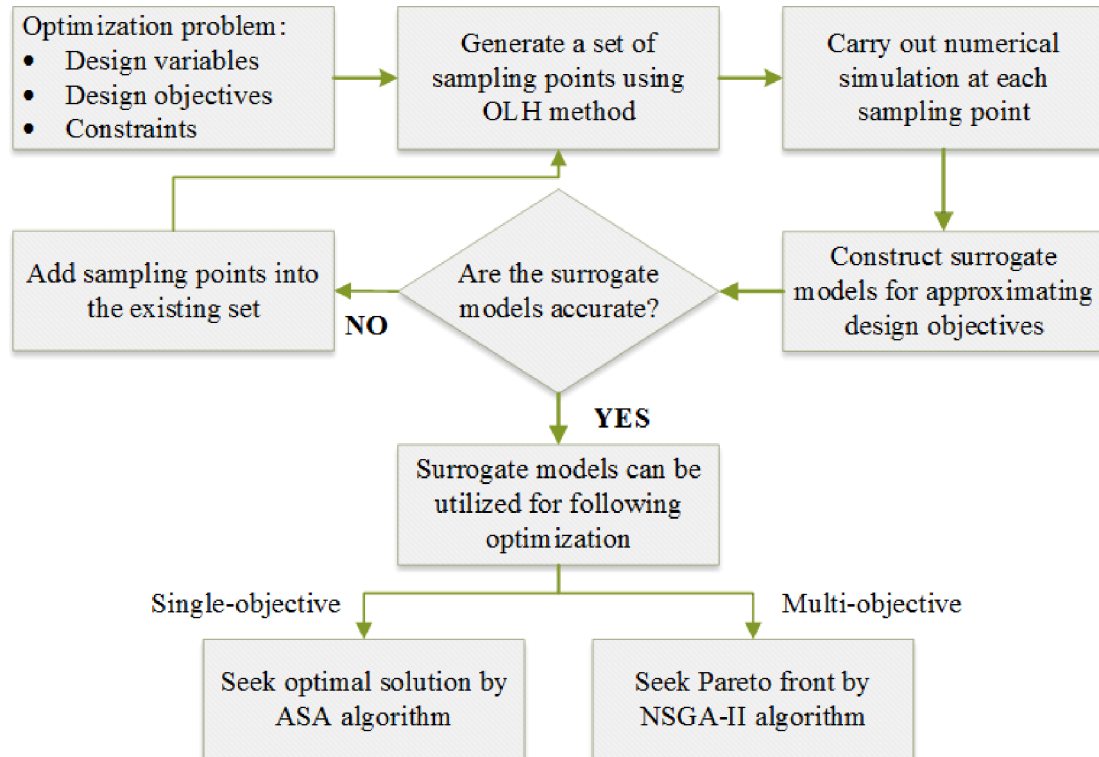


Fig. 13. The flow chart of optimization.

Table 1
Definition of optimization problems.

Case	Definition	Objective	Constraint	Variable
I	Single-objective	min M	$0.2 \text{ mm} < t_{fb} < 1.8 \text{ mm}$ $0.2 \text{ mm} < t_{fc} < 1.8 \text{ mm}$ $1 \text{ mm} < t_p < 10 \text{ mm}$ $D > D_0$ $\eta > \eta_0$	t_{fb} t_{fc} t_p
II	Multi-objective	max D, η	$0.2 \text{ mm} < t_{fb} < 1.8 \text{ mm}$ $0.2 \text{ mm} < t_{fc} < 1.8 \text{ mm}$ $1 \text{ mm} < t_p < 10 \text{ mm}$ $M < M_0$	t_{fb} t_{fc} t_p
III	Multi-objective	max $D/M, \eta/M$	$0.2 \text{ mm} < t_{fb} < 1.8 \text{ mm}$ $0.2 \text{ mm} < t_{fc} < 1.8 \text{ mm}$ $1 \text{ mm} < t_p < 10 \text{ mm}$	t_{fb} t_{fc} t_p

Table 2
Four surrogate models used in this study: parameters and functions.

Surrogate model	Approximation function $\hat{y}(x)$	Refs.
Response surface (RS)	$a_0 + \sum_{i=1}^N b_i x_i + \sum_{ij(i<j)}^N c_{ij} x_i x_j + \sum_{i=1}^N d_i x_i^2 + \sum_{i=1}^N e_i x_i^3$	[46]
Kriging (KRG)	$\hat{\beta} + r^T(x)R^{-1}(y - \hat{\beta}q)$	[47]
Radial basis function (RBF)	$\sum_{i=1}^M \lambda_i \varphi(r(x, x_i)) + \sum_{j=1}^N c_j p_j(x)$	[48]
Orthogonal polynomial (OP)	$a_0 p_0(x) + a_1 p_1(x) + \dots + a_m p_m(x) = \sum_{i=1}^m a_i p_i(x)$	[49]

where y_i, \bar{y}_i and \hat{y}_i are the actual FE-MSE value, the average FE-MSE value and the surrogate model predicted value at these validation points, and M_v is the number of validation points.

Fig. 14 compared the cross-validation results of the four surrogate models, where the actual and predicted results at the validation points were placed on a graph. The black line (1:1 line) shown in Fig. 14 represented perfect agreement of the surrogate model and FE-MSE method. The results with the KRG model (Fig. 14b) exhibited the worst

convergence with respect to the 1:1 line. Further, three quantitative parameters were used to evaluate the accuracy of the surrogate models. As shown in Fig. 15, the OP model exhibited the best accuracy, with the highest values of R^2 and the lowest value of RMSE and MAPE. Hence, the following optimization work was carried out based on the OP model.

5.3. Optimization algorithm

To explore the optimal configuration of the proposed sandwich panel for simultaneous vibration attenuation and structural stiffness, the ASA algorithm [51] for single-objective optimization and the NSGA-II algorithm [52] for multi-objective optimization were employed. The ASA algorithm is well-suited for solving highly nonlinear problems with short running analysis codes when finding the global optimum becomes more important than a quick improvement of the design [51]. Key parameters of the algorithm, including the maximum number of generated designs, the number of designs for convergence check and the convergence epsilon, were set as 50000, 5, and 1.0×10^{-8} , respectively. NSGA-II is a multi-objective genetic algo-

Table 3
Sampling points and FE-MSE predictions at these points.

No.	t_{fb} (mm)	t_{fc} (mm)	t_p (mm)	η (%)	No.	t_{fb} (mm)	t_{fc} (mm)	t_p (mm)	η (%)
1	1.312	1.393	1.150	11.682	31	0.797	1.258	1.310	2.042
2	0.254	0.390	4.970	12.306	32	1.637	1.203	7.250	10.368
3	1.529	0.308	9.850	1.928	33	0.769	0.688	7.860	4.634
4	1.258	0.742	6.950	8.852	34	0.525	0.553	1.610	4.869
5	0.688	0.363	3.900	2.762	35	0.227	1.529	4.200	3.620
6	0.580	0.715	5.580	6.002	36	0.932	0.797	1.000	3.205
7	1.447	0.281	2.980	6.059	37	0.959	0.959	5.270	7.017
8	1.556	0.851	8.930	5.724	38	1.800	1.475	2.530	13.138
9	1.719	1.231	4.660	12.172	39	0.851	0.254	8.630	4.696
10	1.339	1.420	3.750	4.400	40	1.149	1.041	2.680	7.272
11	0.715	0.932	3.140	9.120	41	0.905	1.366	4.050	12.258
12	1.285	0.227	7.560	4.083	42	1.041	1.692	2.370	5.373
13	1.068	1.095	8.170	1.765	43	1.014	0.417	5.880	10.728
14	1.231	1.312	6.190	4.207	44	0.742	1.014	10.000	5.144
15	1.502	1.800	2.830	3.204	45	1.122	1.746	5.120	7.426
16	0.634	1.719	4.360	1.619	46	1.610	1.068	2.220	6.393
17	1.692	0.471	7.710	2.255	47	0.417	1.339	9.080	9.318
18	0.308	0.525	7.410	5.043	48	1.176	0.580	9.240	8.051
19	1.664	1.610	8.320	7.205	49	0.824	1.556	6.800	8.290
20	1.746	0.634	3.290	2.599	50	0.471	1.176	4.810	11.211
21	0.336	1.149	2.070	2.690	51	0.390	1.502	6.640	1.398
22	0.498	0.498	9.690	12.909	52	0.200	0.986	6.490	15.347
23	1.393	1.285	9.540	6.896	53	1.773	0.824	6.030	13.011
24	0.986	0.336	1.760	8.548	54	0.281	0.769	3.440	5.622
25	1.095	0.607	3.590	1.777	55	1.366	0.661	1.460	9.469
26	0.553	1.773	8.470	1.916	56	1.203	1.664	8.020	8.449
27	0.444	1.583	1.920	10.195	57	0.607	0.200	6.340	2.599
28	1.583	1.637	5.730	9.360	58	0.661	1.122	7.100	2.949
29	1.420	0.878	4.510	5.685	59	1.475	0.444	5.420	5.952
30	0.363	0.905	8.780	7.837	60	0.878	1.447	9.390	13.009

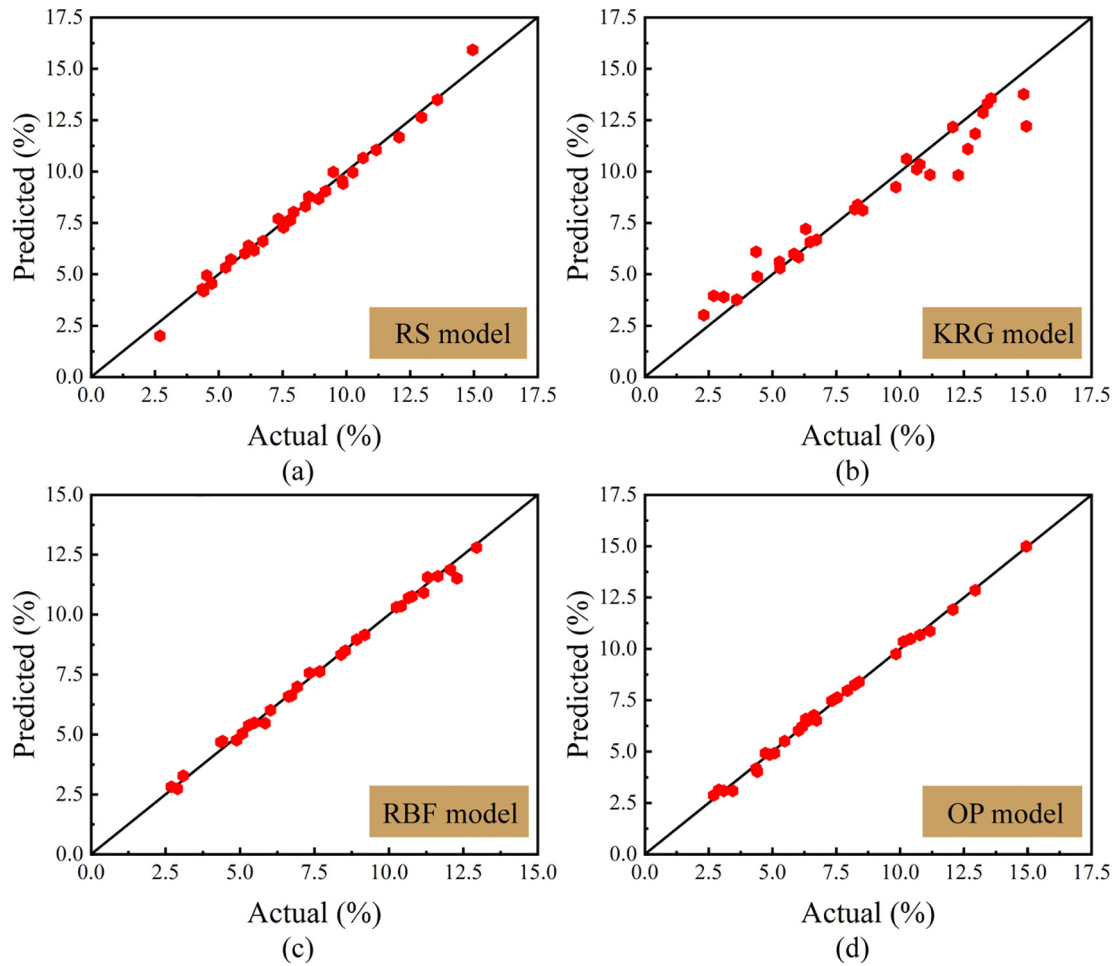


Fig. 14. Cross-validation results of four surrogate models: (a) RS model, (b) KRG model, (c) RBF model, and (d) OP model.

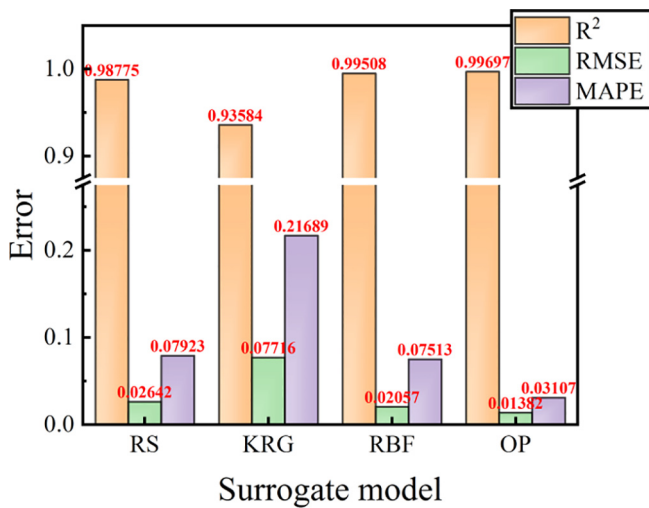


Fig. 15. Error analysis of four surrogate models.

rithm built upon the principle of nondominated sorting and sharing, which enables finding much better spread of solutions and better convergence near the true Pareto-optimal front [52]. Key parameters including the population size, the number of generations, the crossover probability, the crossover distribution index and the mutation distribution index were set as 100, 500, 0.9, 20 and 100, respectively.

5.4. Optimization results

5.4.1. Case I

As listed in Table 4, the sandwich panel was optimized to achieve minimum structural weight while maintaining the same capacity of vibration attenuation and structural stiffness. In contrast with the initial design (specimen S-6), the total mass of the sandwich decreased from 1.595 kg to 1.484 kg, a drop of ~7%. At the optimum point, the design variables (t_{fb} , t_{fb} , t_p) were identified as $t_{fb} = 0.200$ mm, $t_{fc} = 0.809$ mm and $t_p = 1.916$ mm, implying that the constrained metal layer should be more or less thicker than the base metal layer for enhanced performance. To further confirm the accuracy of the surrogate model used in this study, the surrogate based optimum and FE-MSE result of the first damping loss factor η were compared. From Table 4, the prediction of the OP model was only 3.494% higher than the FE-MSE analysis, thus demonstrating that the OP model was sufficiently accurate and could provide reliable predictions of the first damping loss factor.

5.4.2. Case II

This case aimed to achieve optimal performance of structural stiffness and vibration damping at a fixed total mass. The conflict between two design objectives usually leads to a Pareto front where each point represents an optimal design in different situations. As shown in Fig. 16a, the Pareto front of Case II was obtained, and the optimal results in the Pareto front were fitted to a polynomial expression, as:

$$D = 1489070 - 505529\eta + 58583\eta^2 - 2265\eta^3 \quad (20)$$

Table 4
Optimal design results of Case I.

Description	Parameter	Initial design	Optimal design		
			OP model	FE-MSE method	Error (%)
Objective	M (kg)	1.595	1.484	–	–
Constraint	D (Pa m^4)	29467.006	29467.010	–	–
	η (%)	6.634	7.020	6.783	3.494
Variable	t_{fb} (mm)	0.500	0.200	–	–
	t_{fc} (mm)	0.500	0.809	–	–
	t_p (mm)	3.000	1.916	–	–

where the R-square of the polynomial fitting was 0.9985. In order to compare with the preliminary sandwich design, the Pareto front was processed and redrawn in the form of enhancement ratio. As shown in Fig. 16b, the two design objectives (i.e., D and η) of the optimal designs exhibited significant enhancement of 5.849–13.772% and 26.564–43.452%, respectively. A spatial distribution of optimum points in the design space was also obtained, as shown in Fig. 16c. The design variables (t_{fb} , t_{fc} , t_p) at these points ranged in $0.2 \text{ mm} < t_{fb} < 0.20011 \text{ mm}$, $0.56951 \text{ mm} < t_{fc} < 0.81276 \text{ mm}$ and $2.85263 \text{ mm} < t_p < 4.78169 \text{ mm}$, respectively. These results suggested that the base metal layer was expected to be thin, and proper combination of the constrained metal layer and polyurea layer could lead to a

more desirable performance. Finally, to verify the accuracy and effectiveness of the present optimization, the FE-MSE predictions for three representative points (marked in Fig. 16a) were separately obtained. Table 5 compared the FE-MSE predictions with the optimization results on the first damping loss factor η .

5.4.3. Case III

Exploring a higher structural efficiency of flexural stiffness and vibration damping continues to be technically important for designing multi-functional lightweight sandwich structures. Therefore, this case chose the specific flexural stiffness D/M and the specific damping loss factor η/M as design objectives. Similar to case II, a Pareto front was

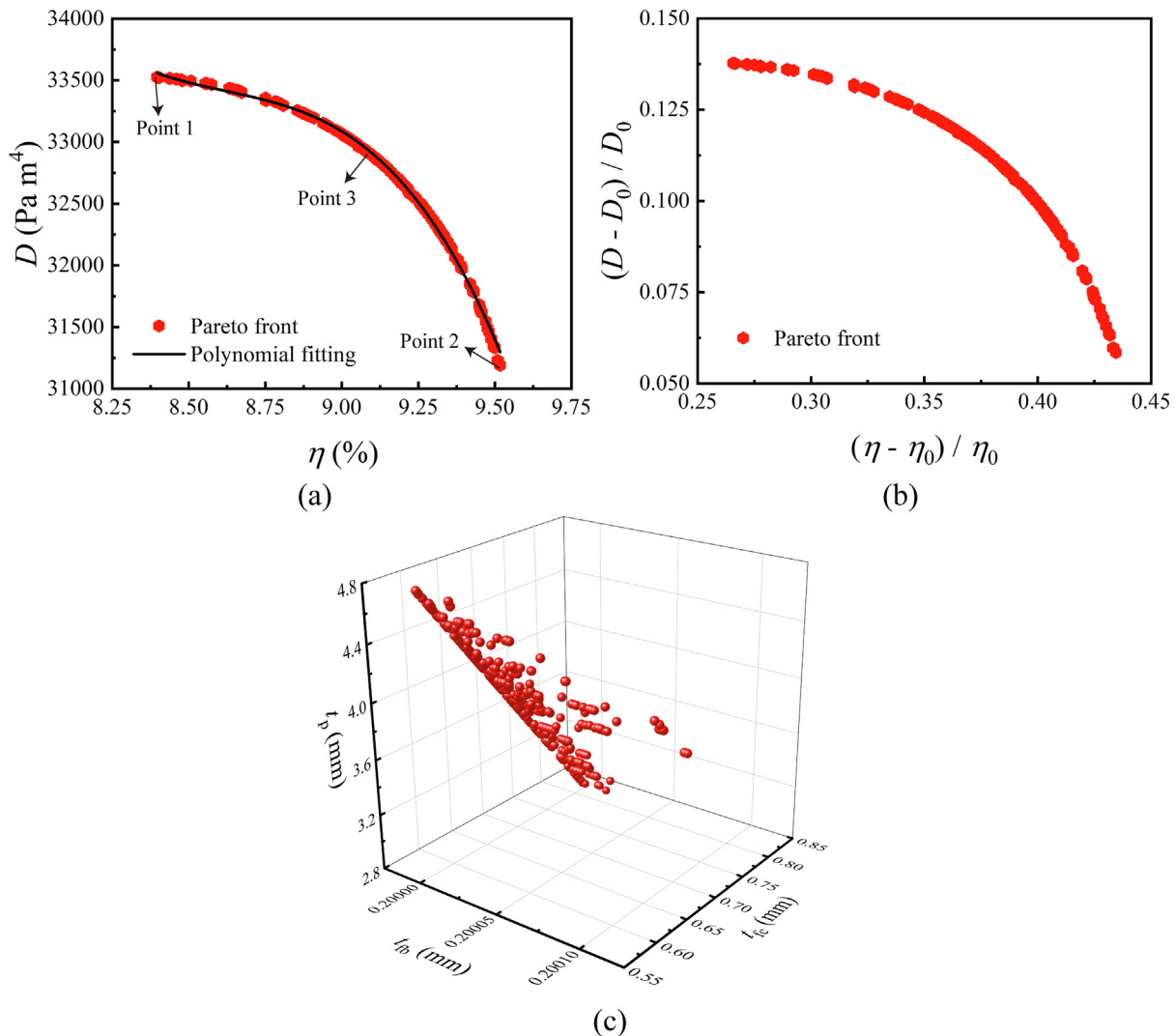


Fig. 16. Optimal design results of Case II: (a) Pareto front, (b) enhancement ratio of Pareto front, and (c) spatial distribution of optimum points.

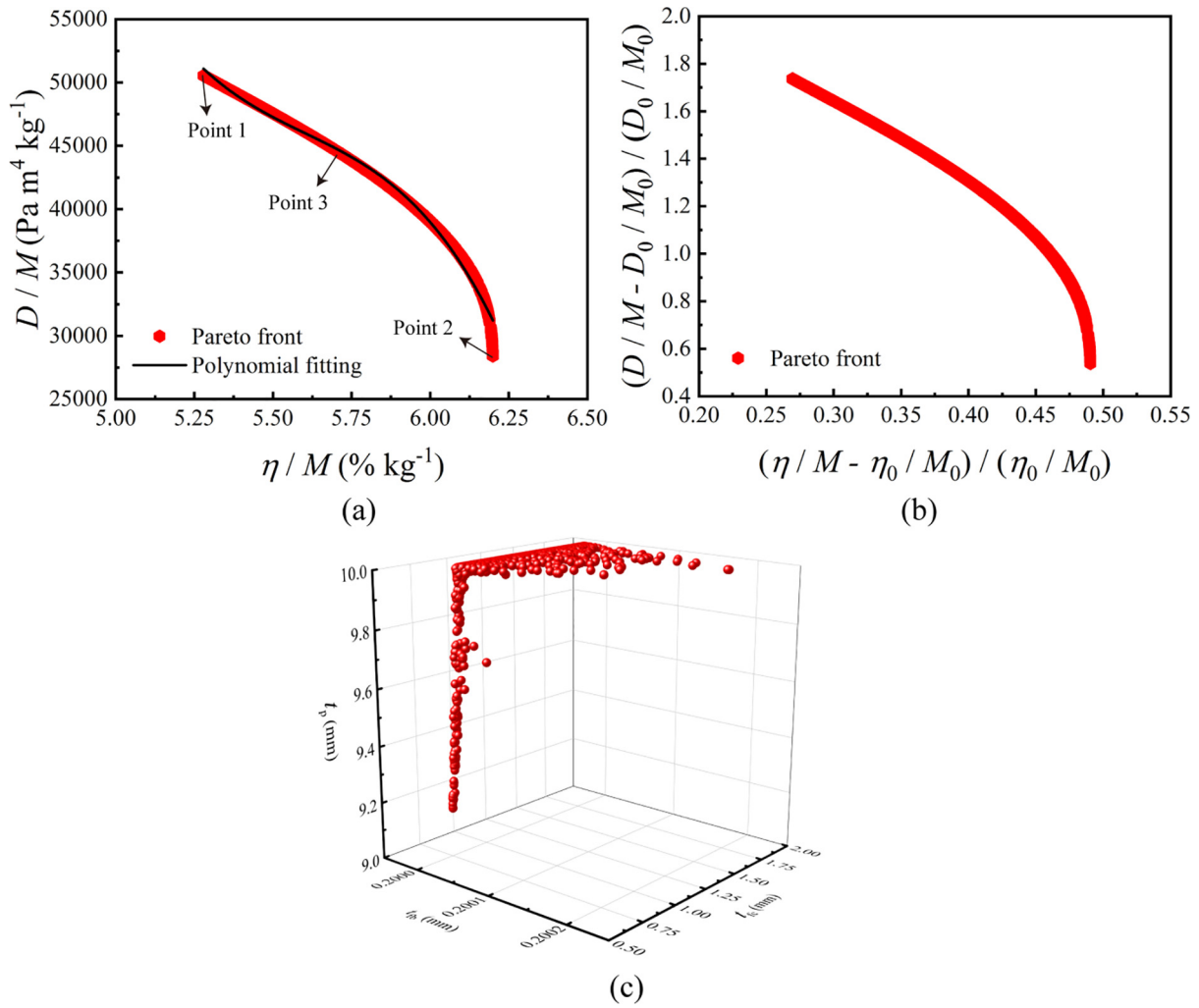


Fig. 17. Optimal design results of Case III: (a) Pareto front, (b) enhancement ratio of Pareto front, and (c) spatial distribution of optimum points.

Table 5
Comparison between FE-MSE predictions and optimization solutions of Case II.

Specimen	t_{fb} (mm)	t_{fc} (mm)	t_p (mm)	M (kg)	D (Pa m ⁴)	η (%)		
						OP model	FE-MSE method	Error (%)
Point 1	0.200	0.813	2.853	1.590	33525.392	8.397	8.287	1.330
Point 2	0.200	0.696	3.780	1.590	31190.462	9.517	9.401	1.235
Point 3	0.200	0.570	4.782	1.590	32914.002	9.088	8.988	1.109

Table 6
Comparison between FE-MSE predictions and optimization solutions of Case III.

Specimen	t_{fb} (mm)	t_{fc} (mm)	t_p (mm)	D/M (Pa m ⁴ kg ⁻¹)	η/M (% kg ⁻¹)		
					OP model	FE-MSE method	Error (%)
Point 1	0.200	1.800	10.000	50521.952	5.279	5.424	-2.673
Point 2	0.200	0.759	9.173	28513.468	6.199	6.031	2.786
Point 3	0.200	1.440	10.000	44397.150	5.708	5.913	-3.467

obtained (Fig. 17a), which was then compared with the preliminary design (Fig. 17b). Optimal designs in the Pareto front could be fitted by a polynomial given by:

$$\frac{D}{M} = 6408790 - 3382900\left(\frac{\eta}{M}\right) + 601640\left(\frac{\eta}{M}\right)^2 - 35794\left(\frac{\eta}{M}\right)^3 \quad (21)$$

where the R-square of the polynomial fitting was 0.9933. As shown in Fig. 17b, the two design objectives (i.e. D/M and η/M) of the optimal designs achieved a remarkable increase of 53.789–173.63% and 26.927–49.046%, respectively. Fig. 17c displayed the corresponding spatial distribution of design variables in the Pareto front, as

0.2 mm < t_{fb} < 0.20021 mm, 0.75913 mm < t_{fc} < 1.8 mm and 9.17278 mm < t_p < 10 mm. Finally, to verify the accuracy and effectiveness of the present optimization, the FE-MSE predictions for three representative points (marked in Fig. 17a) were separately carried out. Table 6 compared the FE-MSE predictions with the optimization results on the specific damping loss factor η/M .

6. Concluding remarks

With focus placed upon laser-welded corrugated-core (LASCOR) sandwich panels with polyurea-metal laminate face sheets (PML) face sheets, this study aimed to reveal the sensitivity of the vibration damping characteristics and propose a multi-objective optimization framework factoring vibration attenuation, structural stiffness and total weight of these novel multifunctional sandwich constructions. For enhanced calculation efficiency, surrogate modeling was validated and implemented into the optimization procedure. Main findings were summarized as follows.

- (i) The natural frequencies and damping loss factors of the sandwich panels displayed different sensitivities to key geometric parameters, and significantly outperformed monolithic panels of equal mass.
- (ii) Under the principles of cross-validation, the orthogonal polynomial (OP) model provided the most accurate approximation for damping loss factors.
- (iii) Upon coupling the surrogate model with the optimization algorithm, a high-efficiency multi-objective optimization framework factoring stiffness, damping and weight of LASCOR sandwich panels with PML face sheets was proposed.
- (iv) For single-objective optimization, the structural weight of the optimized sandwich panel decreased by around 7% in contrast with the initial design. For multi-objective optimizations, the Pareto fronts revealed significant enhancement in both the damping loss factor/structural stiffness and specific damping loss factor/structural stiffness.

CRedit authorship contribution statement

Xin Wang: Conceptualization, Methodology, Writing - original draft, Writing - review & editing. **Xue Li:** Investigation, Data curation. **Zeng-Shen Yue:** Investigation, Software. **Run-Pei Yu:** Methodology. **Qian-Cheng Zhang:** Formal analysis, Writing - review & editing. **Shao-Feng Du:** Validation. **Zhi-Kun Yang:** Resources. **Bin Han:** Investigation. **Tian Jian Lu:** Supervision, Conceptualization, Funding acquisition, Writing - review & editing.

Declaration of Competing Interest

The authors declare that they have no known competing financial interests or personal relationships that could have appeared to influence the work reported in this paper.

Acknowledgments

This work was supported by National Key Research and Development Program of China (2017YFB1102801), National Natural Science Foundation of China (12072250, 11972185, 12002156 and 11902148), China Postdoctoral Science Foundation (2020M671473), Open Project for Key Laboratory of Intense Dynamic Loading and Effect (KLIDLE1801), Aviation Science Foundation Project (20170970002), Natural Science Fund Project in Jiangsu Province (BK20190392), and Open Fund of State Key Laboratory of Mechanics and Control of Mechanical Structures (MCMS-E0219K02 and MCMS-I-0219 K01) and State Key Laboratory of Smart Manufacturing for

Special Vehicles and Transmission System (GZ2019KF015). XW and XL would like to thank Sheng-Fa Zhu (a top programmer in SenseTime) for several insightful discussions about the surrogate-based optimization.

References

- [1] Zhang Q, Yang X, Li P, Huang G, Feng S, Shen C, et al. Bioinspired engineering of honeycomb structure - Using nature to inspire human innovation. *Prog Mater Sci* 2015;74:332–400. <https://doi.org/10.1016/j.pmatsci.2015.05.001>.
- [2] Lu TJ, Valdevit L, Evans AG. Active cooling by metallic sandwich structures with periodic cores. *Prog Mater Sci* 2005;50:789–815. <https://doi.org/10.1016/j.pmatsci.2005.03.001>.
- [3] Tang Y, Li F, Xin F, Lu TJ. Heterogeneously perforated honeycomb-corrugation hybrid sandwich panel as sound absorber. *Mater Des* 2017;134:502–12. <https://doi.org/10.1016/j.matdes.2017.09.006>.
- [4] Wang X, Yu RP, Zhang QC, Li L, Li X, Zhao ZY, et al. Dynamic response of clamped sandwich beams with fluid-filled corrugated cores. *Int J Impact Eng* 2020;139:. <https://doi.org/10.1016/j.ijimpeng.2020.103533>.
- [5] Ni CY, Li YC, Xin FX, Jin F, Lu TJ. Ballistic resistance of hybrid-cored sandwich plates: Numerical and experimental assessment. *Compos Part A Appl Sci Manuf* 2013;46:69–79. <https://doi.org/10.1016/j.compositesa.2012.07.019>.
- [6] Lakes RS. High damping composite materials. *J Compos Mater* 2008;36:287–97. <https://doi.org/10.1106/002199802023538>.
- [7] Ashby MF. Materials selection in mechanical design. fifth ed. Butterworth-Heinemann; 2017. https://doi.org/10.1007/978-3-319-05203-8_21.
- [8] Kerwin Jr EM. Damping of flexural waves by a constrained viscoelastic layer. *J Acoust Soc Am* 1959;31:952–62.
- [9] Oberst H, Frankenfeld K. Über die Dämpfung der Biegeschwingungen dünner Bleche durch fest haftende Beläge. *Acta Acust United with Acust* 1952;2:181–94.
- [10] Kerwin Jr EM. Macromechanisms of damping in composite structures. In: Lazan BJ, editor. Intern. frict. damping, cycl. plast., West Conshohocken, PA: ASTM International; 1965, p. 125–49. <https://doi.org/10.1520/STP43767S>.
- [11] Ege K, Roozen NB, Leclère Q, Rinaldi RG. Assessment of the apparent bending stiffness and damping of multilayer plates; modelling and experiment. *J Sound Vib* 2018;426:129–49. <https://doi.org/10.1016/j.jsv.2018.04.013>.
- [12] Guyader JL, Lesueur C. Acoustic transmission through orthotropic multilayered plates, part II: transmission loss. *J Sound Vib* 1978;58:69–86. [https://doi.org/10.1016/S0022-460X\(78\)80061-3](https://doi.org/10.1016/S0022-460X(78)80061-3).
- [13] Guyader JL, Cacciolati C. Viscoelastic properties of single layer plate material equivalent to multi-layer composites plate. In: 36th int. congr. exhib. noise control eng., vol. 3; 2007. p. 1558–67.
- [14] Ross D, Ungar EE, Kerwin EM. Damping of plate flexural vibrations by means of viscoelastic laminae. *Struct Damping* 1960:49–87.
- [15] Viktorov I. Rayleigh and lamb waves; 1967.
- [16] Hui Y, Giunta G, Belouettar S, Huang Q, Hu H, Carrera E. A free vibration analysis of three-dimensional sandwich beams using hierarchical one-dimensional finite elements. *Compos Part B Eng* 2017;110:7–19. <https://doi.org/10.1016/j.compositesb.2016.10.065>.
- [17] Huang Q, Liu Y, Hu H, Shao Q, Yu K, Giunta G, et al. A Fourier-related double scale analysis on the instability phenomena of sandwich plates. *Comput Methods Appl Mech Eng* 2017;318:270–95. <https://doi.org/10.1016/j.cma.2017.01.021>.
- [18] Yu K, Hu H, Tang H, Giunta G, Potier-Ferry M, Belouettar S. A novel two-dimensional finite element to study the instability phenomena of sandwich plates. *Comput Methods Appl Mech Eng* 2015;283:1117–37. <https://doi.org/10.1016/j.cma.2014.08.006>.
- [19] Boumediene F, Daya EM, Cadou JM, Duigou L. Forced harmonic response of viscoelastic sandwich beams by a reduction method. *Mech Adv Mater Struct* 2016;23:1290–9. <https://doi.org/10.1080/15376494.2015.1068408>.
- [20] Hamdaoui M, Akoussan K, Daya EM. Comparison of non-linear eigensolvers for modal analysis of frequency dependent laminated visco-elastic sandwich plates. *Finite Elem Anal Des* 2016;121:75–85. <https://doi.org/10.1016/j.finel.2016.08.001>.
- [21] Yang JS, Xiong J, Ma L, Wang B, Zhang GQ, Wu LZ. Vibration and damping characteristics of hybrid carbon fiber composite pyramidal truss sandwich panels with viscoelastic layers. *Compos Struct* 2013;106:570–80. <https://doi.org/10.1016/j.compstruct.2013.07.015>.
- [22] Yang JS, Xiong J, Ma L, Zhang GQ, Wang XT, Wu LZ. Study on vibration damping of composite sandwich cylindrical shell with pyramidal truss-like cores. *Compos Struct* 2014;117:362–72. <https://doi.org/10.1016/j.compstruct.2014.06.042>.
- [23] Yang JS, Xiong J, Ma L, Feng LN, Wang SY, Wu LZ. Modal response of all-composite corrugated sandwich cylindrical shells. *Compos Sci Technol* 2015;115:9–20. <https://doi.org/10.1016/j.compscitech.2015.04.015>.
- [24] Wang X, Li X, Yu RP, Ren JW, Zhang QC, Zhao ZY, et al. Enhanced vibration and damping characteristics of corrugated sandwich panels with polyurea-metal laminate face sheets. *Compos Struct* 2020;251:. <https://doi.org/10.1016/j.compstruct.2020.112591>.
- [25] Yang JS, Ma L, Schmidt R, Qi G, Schröder KU, Xiong J, et al. Hybrid lightweight composite pyramidal truss sandwich panels with high damping and stiffness efficiency. *Compos Struct* 2016;148:85–96. <https://doi.org/10.1016/j.compstruct.2016.03.056>.
- [26] Aumjaud P, Fieldsend JE, Boucher MA, Evans KE, Smith CW. Multi-objective optimisation of viscoelastic damping inserts in honeycomb sandwich structures.

- Compos Struct 2015;132:451–63. <https://doi.org/10.1016/j.compstruct.2015.05.061>.
- [27] Aumjaud P, Smith CW, Evans KE. A novel viscoelastic damping treatment for honeycomb sandwich structures. *Compos Struct* 2015;119:322–32. <https://doi.org/10.1016/j.compstruct.2014.09.005>.
- [28] Wang GG, Shan S. Review of metamodeling techniques in support of engineering design optimization. *J Mech Des Trans ASME* 2007;129:370–80. <https://doi.org/10.1115/1.2429697>.
- [29] Fang J, Sun G, Qiu N, Kim NH, Li Q. On design optimization for structural crashworthiness and its state of the art. *Struct Multidiscip Optim* 2017;55:1091–119. <https://doi.org/10.1007/s00158-016-1579-y>.
- [30] Yang M, Han B, Su PB, Wei ZH, Zhang Q, Zhang QC, et al. Axial crushing of ultralight all-metallic truncated conical sandwich shells with corrugated cores. *Thin-Walled Struct* 2019;140:318–30. <https://doi.org/10.1016/j.tws.2019.03.048>.
- [31] Wang E, Li Q, Sun G. Computational analysis and optimization of sandwich panels with homogeneous and graded foam cores for blast resistance. *Thin-Walled Struct* 2020;147. <https://doi.org/10.1016/j.tws.2019.106494>106494.
- [32] Wang X, Zhao ZY, Li L, Zhang ZJ, Zhang QC, Han B, et al. Free vibration behavior of Ti-6Al-4V sandwich beams with corrugated channel cores: experiments and simulations. *Thin-Walled Struct* 2019;135:329–40. <https://doi.org/10.1016/j.tws.2018.11.008>.
- [33] Johnson CD, Kienholz DA. Finite element prediction of damping in structures with constrained viscoelastic layers. *AIAA J* 1982;20:1284–90.
- [34] Ghorbel A, Akrouf A, Abdennadher M, Bouzouane B, Boukharouba T, Haddar M. Ultra-thin films inter-facial shear effects on modal damping characterization of laminated plate. *Appl Acoust* 2017;128:71–82. <https://doi.org/10.1016/j.apacoust.2017.01.008>.
- [35] Montemurro M, Koutsawa Y, Belouettar S, Vincenti A, Vannucci P. Design of damping properties of hybrid laminates through a global optimisation strategy. *Compos Struct* 2012;94:3309–20. <https://doi.org/10.1016/j.compstruct.2012.05.003>.
- [36] Madigosky WM, Lee GF, Niemiec JM. A method for modeling polymer viscoelastic data and the temperature shift function. *J Acoust Soc Am* 2006;119:3760–5. <https://doi.org/10.1121/1.2195292>.
- [37] Butcher EA, Segalman DJ. Characterizing damping and restitution in compliant impacts via modified k-v and higher-order linear viscoelastic models. *J Appl Mech Trans ASME* 2000;67:831–4. <https://doi.org/10.1115/1.1308578>.
- [38] Chandra R, Singh SP, Gupta K. Damping studies in fiber-reinforced composites – a review. *Compos Struct* 1999;46:41–51. [https://doi.org/10.1016/S0263-8223\(99\)00041-0](https://doi.org/10.1016/S0263-8223(99)00041-0).
- [39] Sayyad AS, Ghugal YM. Bending, buckling and free vibration of laminated composite and sandwich beams: a critical review of literature. *Compos Struct* 2017;171:486–504. <https://doi.org/10.1016/j.compstruct.2017.03.053>.
- [40] Timoshenko SP. On the correction for shear of the differential equation for transverse vibrations of prismatic bars. *Philos Mag* 1921;41:744–6. <https://doi.org/10.1080/14786442108636264>.
- [41] Zhang ZJ, Han B, Zhang QC, Jin F. Free vibration analysis of sandwich beams with honeycomb-corrugation hybrid cores. *Compos Struct* 2017;171:335–44. <https://doi.org/10.1016/j.compstruct.2017.03.045>.
- [42] Derby TF, Ruzicka JE. Loss factor and resonant frequency of viscoelastic shear-damped structural composites; 1969.
- [43] Liu T, Deng ZC, Lu TJ. Design optimization of truss-cored sandwiches with homogenization. *Int J Solids Struct* 2006;43:7891–918. <https://doi.org/10.1016/j.ijsolstr.2006.04.010>.
- [44] Liu T, Deng ZC, Lu TJ. Structural modeling of sandwich structures with lightweight cellular cores. *Acta Mech Sin Xuebao* 2007;23:545–59. <https://doi.org/10.1007/s10409-007-0096-z>.
- [45] Park J. Optimal Latin-hypercube experiments. *J Stat Plan Inference* 1994;39:95–111.
- [46] Khuri AI, Cornell JA. Response surfaces: designs and analyses. Second Edi: CRC Press; 2018.
- [47] Sacks J, Welch WJ, Mitchell TJ, Wynn HP. Design and analysis of computer experiments. *Stat Sci* 1989;4:409–23. <https://doi.org/10.1214/ss/1177012420>.
- [48] Hardy RL. Multiquadric equations of topography and other irregular surfaces. *J Geophys Res* 1971;76:1905–15. <https://doi.org/10.1029/jb076i008p01905>.
- [49] Narula SC. Orthogonal polynomial regression. *Int Stat Rev Int Stat* 1979:31–6.
- [50] Browne MW. Cross-validation methods. *J Math Psychol* 2000;44:108–32. [https://doi.org/10.1016/S0309-1740\(01\)00042-0](https://doi.org/10.1016/S0309-1740(01)00042-0).
- [51] Ingber L. Adaptive simulated annealing (ASA): lessons learned. *Control Cybern* 1996;25:32–54.
- [52] Deb K, Pratap A, Agarwal S, Meyarivan T. A fast and elitist multiobjective genetic algorithm: NSGA-II. *IEEE Trans Evol Comput* 2002;6:182–97. <https://doi.org/10.1109/4235.996017>.